China Geology 8 (2025) 117−140

China Geology

Journal homepage: http://chinageology.cgs.cn
https://www.sciencedirect.com/journal/china-geology

Assessment of ecological geological vulnerability in Mu Us Sandy Land based on GIS and suggestions of ecological protection and restoration

Jian-yu Liu[a], Hong-feng Nie[a,*], Liang Xu[b], Chun-lei Xiao[a], Wei Li[a], Guo-li Yuan[b], Yan-peng Huang[b], Xin-yang Ji[a], Tian-qi Li[a]

[a] *China Aero Geophysical Survey & Remote Sensing Center for Natural Resources, China Geological Survey, Ministry of Natural Resources, Beijing* 100083, *China*
[b] *China University of Geosciences (Beijing), Beijing* 100083, *China*

ARTICLE INFO

Article history:
Received 8 March 2023
Received in revised form 11 November 2023
Accepted 1 December 2023
Available online 21 March 2024

Keywords:
Eco-geological vulnerability
Analytic hierarchy process
Entropy weight method
Evaluation and zonation
Mu Us Sandy Land
Geology-meteorology-soil-topography-vegetation
Precipitation and groundwater
Environmental protection and restoration
Environmental restoration engineering
Inner Mongolia Plateau

ABSTRACT

Eco-geological vulnerability assessment is a significant research topic within the field of eco-geology, but it remains poorly studied. The Mu Us Sandy Land, located in the central part of the farming-pastoral ecotone in northern China, plays a critical role in maintaining the ecological security pattern in this region. However, this sandy land also faces severe sandy desertification and ecological degradation. This study conducted a regional eco-geological vulnerability assessment of the Mu Us Sandy Land using a comprehensive index evaluation method based on eco-geological theories and survey results. To construct an appropriate index system for the eco-geological vulnerability assessment of the Mu Us Sandy Land, the study considered the sandy land's unique characteristics and identified 15 factors of five categories, namely geology, meteorology, soil, topography, and vegetation. The paper calculated the comprehensive weights of all the indices using the analytic hierarchy process (AHP) and the entropy weight method (EWM). Furthermore, it established the eco-geological vulnerability index (EGVI) and obtained the assessment results. The results showed that the eco-geological vulnerability of the Mu Us Sandy Land gradually intensifies from east to west, manifested as vulnerable eco-geological conditions overall. Specifically, extremely vulnerable zones are found in the northwestern and southeastern parts of the study area, highly vulnerable zones in the western and southern parts, moderately vulnerable zones in the central part, and slightly and potentially vulnerable zones in the eastern and southern parts. Areas with high spatial autocorrelations include the northern Uxin Banner - Otog Banner - Angsu Town area, the surrounding areas of Hongdunjie Town in the southeastern part of the study area, the Hongshiqiao Township - Xiaohaotu Township area, Otog Front Banner, and Bainijing Town, which should be prioritized in the ecological conservation and restoration. Additionally, the paper proposed suggestions for the ecological conservation and restoration of county-level administrative areas in the study area. Overall, the findings provide a valuable reference for the ecological conservation and restoration of the Mu Us Sandy Land and other desert areas in arid and semi-arid regions.

1. Introduction

The concept of vulnerability, originally developed in natural disaster research (Martin V, 2008; Dückers M et al., 2015), has been widely applied in various areas such as climate change (Shahbazi F et al., 2009; Buotte PC et al., 2016), land use changes (Santos RG et al., 2015; Huang YF et al., 2012), and social sciences (Frigerio I et al., 2016; Lee YJ, 2014). The concept of ecological vulnerability can be traced back to the early 20th century when the ecologist Clements introduced the concept of ecotone. According to Timmerman P (1981), vulnerability is the degree to which a system produces an unfavorable response when a disaster occurs. Turner BL et al. (2003) pointed out that, vulnerability is the degree to which a system, subsystem, or system component is likely to experience harm due to exposure to a hazard, either a perturbation or stress/stressor. Williams LR et al. (2000) believed that ecosystem vulnerability is the potential of an ecosystem to modulate its response to stressors over time and space. Adger WN (2006) defined vulnerability as the state of

First author: *E-mail address*: liujy5577@163.com (Jian-yu Liu).

* Corresponding author: *E-mail address*: nie_hongfeng@qq.com (Hong-feng Nie).

Literary editor: Li-qiong Jia
doi:10.31035/cg20230027
2096-5192/© 2025 China Geology Editorial Office.

susceptibility to harm from exposure to stresses associated with environmental and social change and from the absence of capacity to adapt. These scholars agreed that vulnerability is an intrinsic attribute of ecosystems and is used to describe the degree of susceptibility to external stresses.

Ecological vulnerability has been a hot topic in ecological research, and significant progress has been made in evaluating ecological vulnerability in recent years. Two main methods are commonly used: Single index methods and comprehensive index methods. The former is mainly employed to evaluate critical factors (Shao HY et al., 2016; Tánago IG et al., 2016; Jewitt D et al., 2015). By comparison, for comprehensive index methods, it is necessary to establish an assessment index system and calculate the weights of various factors using mathematical methods (Li PX et al., 2014; Hong WY et al., 2016; He L et al., 2018; Xue LQ et al., 2019; Hu XJ et al., 2021). However, geological factors are often overlooked in ecological vulnerability assessments, and they are rarely incorporated into the assessment index systems.

Eco-geology, as a new branch of geology and a special research field, is an emerging interdisciplinary science connecting ecology and geology. Its research scope includes the geoscience mechanisms, geological processes, and environmental conditions of ecological problems or ecological processes. It integrates ecological spatial distribution patterns, ecological problems, and their changing laws with geological processes to research the impact of the lithosphere, pedosphere, hydrosphere, atmosphere, and biosphere at different levels and dimensions (Trofimov VT, 2001; 2004; 2008; Wang CS et al., 1997; He ZW et al., 2003; Nie HF et al., 2021a). Vulnerability, as a hot topic of ecology, is an essential research aspect of eco-geology in essence. Based on the connotations of ecological vulnerability and eco-geology, the authors consider that eco-geological vulnerability is an attribute of the Earth's surface system in a certain range that the system is susceptible to adverse effects when it is subjected to external stresses or its internal conditions change, with the susceptibility determined by the system's eco-geological conditions, including soil parent materials, geological structures, topography, soils, meteorology, hydrology. This definition inherits the viewpoint that vulnerability is an essential attribute of ecosystems and incorporates eco-geological research ideas. Compared with ecological vulnerability, eco-geological vulnerability emphasizes the relationship between epigenetic geological processes and ecosystems and focuses on the evaluation of natural factors rather than social and economic factors, such as GDP and per capita income (Li PX et al., 2014; Xue LQ et al., 2019).

The eco-geological survey is to investigate the geoscience mechanisms, geological processes, and background conditions of various ecological problems or ecological processes under the guidance of the earth system science theory (Nie HF et al., 2021b). Significant progress has been made in the development of methods for conducting eco-geological surveys, analyzing eco-geological conditions, and evaluating land suitability (Liu ZX et al., 2020; Wang JB et al., 2020; Ma Z et al., 2021; Zhang JH et al., 2021a). Eco-geology related assessment is a primary eco-geological survey task. However, there is currently a lack of studies and reports on the evaluation and zonation of regional eco-geological vulnerability.

The Mu Us Sandy Land suffers from severe sandy desertification and exhibits different meteorological, geological, and geomorphological conditions. Furthermore, no eco-geological vulnerability assessment has been conducted in this sandy land. Hence, this study established an eco-geological vulnerability assessment index system for the Mu Us Sandy Land by integrating various factors and utilizing a geographic information system (GIS) along with the Analytic Hierarchy Process (AHP) and the Evidential Weighted Method (EWM), this study conducted a quantitative assessment of eco-geological vulnerability and investigated spatial autocorrelation. In addition, the study put forward suggestions for the ecological conservation and restoration of the sandy land in response to its sandy desertification. The findings aim to provide a theoretical basis for local ecological conservation and restoration and contribute to further research in relevant fields.

2. Overview of the study area

2.1. Geographical location and topography

The Mu Us Sandy Land, which located at the intersection of Inner Mongolia, Shaanxi, and Ningxia (Fig. 1), is a transitional area between the Ordos and Loess plateaus, including the southern part of Ordos City, the northwestern part of Yulin City, and the northeastern part of Wuzhong City. It is higher in the northwest and lower in the southeast, inclining from northwest to southeast. The predominant landform in the Mu Us Sandy Land is the semi-fixed barchans, which are crescent-shaped sand dunes with heights ranging from 5 m to 15 m. On the southern margin of the sandy land, there is a transitional zone composed of a mix of sand and loess. During the Quaternary Upper Pleistocene, the Mu Us Sandy Land experienced a prolonged period of dry climate, leading to desiccation and denudation. As a result, the ancient fluvial-lacustrine sand beds were exposed and left uncovered. The strong northwest winds that blew in the region carried and deposited sands, gradually shaping the modern topography of the sandy land. This topography is characterized by an alternating distribution of tablelands, sand dunes and depressions.

2.2. Soil parent materials

Within the Mu Us Sandy Land, tablelands are composed primarily of Cretaceous purplish-red sandstones and Jurassic grayish-green sandstones, and depressions are dominated by thick Pleistocene fluvial-lacustrine sediments. During the dry period of the last glacial period, extensive sand drift activity occurred, transforming the Pleistocene sediments into vast

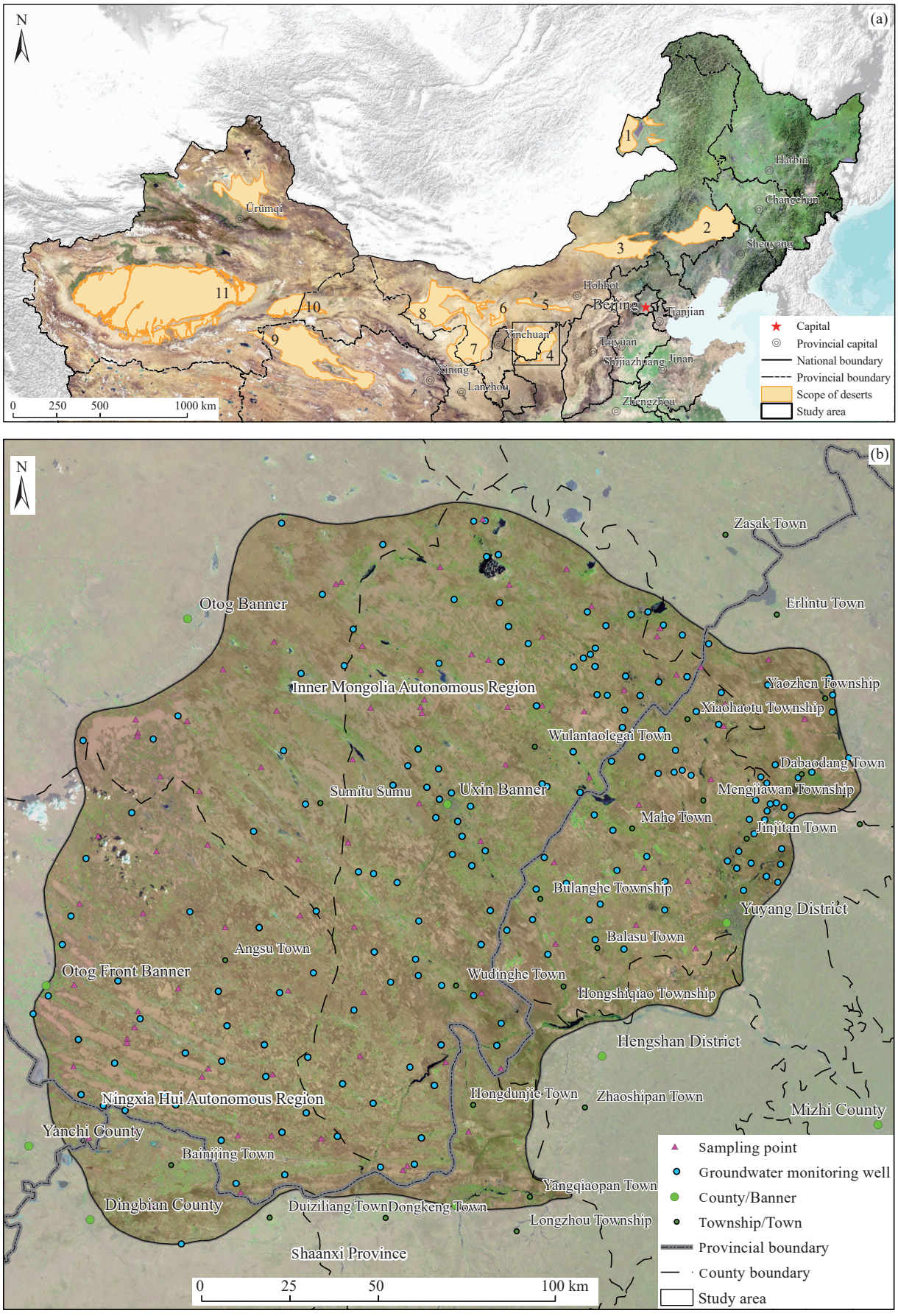

Fig. 1. a–Locations of desserts and sandy land in northern China; b–map of the distribution of survey sites. 1–Hulun Buir sandy land; 2–Horqin sandy land; 3–Hunshandake sandy land; 4–Mu Us sandy land; 5– Kubuqi desert; 6–Ulan Buh desert; 7–Tengger desert; 8–Badain Jaran desert; 9–Qaidam desert; 10–Kumutage desert; 11–Taklamakan desert; 12–Gurbantunggut desert.

aeolian sediments. The present surface of the sandy land is predominantly composed of Quaternary aeolian sediments, as well as fluvial and lacustrine deposits (Liu QQ et al., 2018). The clastic rocks, aeolian sediments, and alluvial-proluvial sediments are overlaid by different soil types, as well as varied types and growth conditions of vegetation.

Based on the survey results and the petrological classification system, as well as the classification system of Quaternary sediments and the genetic classification system of soils, the study divided the soil parent materials by following the fundamental information classification principles such as scientificity, completeness, systematicity, and specificity. Specifically, the soil parent materials were divided into four levels, namely types, categories, groups, and materials (rocks) from high to low (to be published). According to these classification criteria, the study area contains two types of exposed soil parent materials: Loose deposits and deposits insusceptible to weathering; and five categories: Alluvial and proluvial deposits, aeolian sands, loess, lacustrine and paludal deposits, and siliceous (calcareous) sandstones and conglomerates. Among them, aeolian sands cover the largest area of 26378.39 km^2, which accounts for 80.33% of the study area. The aeolian sands are followed by lacustrine and paludal deposits with an area accounting for 14.84% of the study area (Fig. 2; Table 1).

2.3. Vegetation

At present, the vegetation in the Mu Us Sandy Land can be roughly divided into three zones and three groups. From northwest to southeast, the vegetation shifts from the desert steppe to the typical steppe and then to the forest steppe. The typical steppe covers the largest area, accounting for over 90% of the sandy land area (Zhang L, 2021). In the typical steppe zone, the dominant species are *Stipa bungeana* and *Stipa breviflora*, In the desert steppe zone, the predominant species include *Stipa gobica*, *Stipa glareosa*, *Caragana stenphylla*, and *Caragana tibetica* (Li ZX et al., 2005). The three major vegetation groups in the Mu Us Dessert are as follows: (1) Steppes and shrubs on the tablelands, (2) psammophytic vegetation on fixed and semi-fixed sand dunes and sandy land, and (3) meadows, halophilic, and swamp vegetation in the depression. Their primary vegetation formations are presented in Table 2.

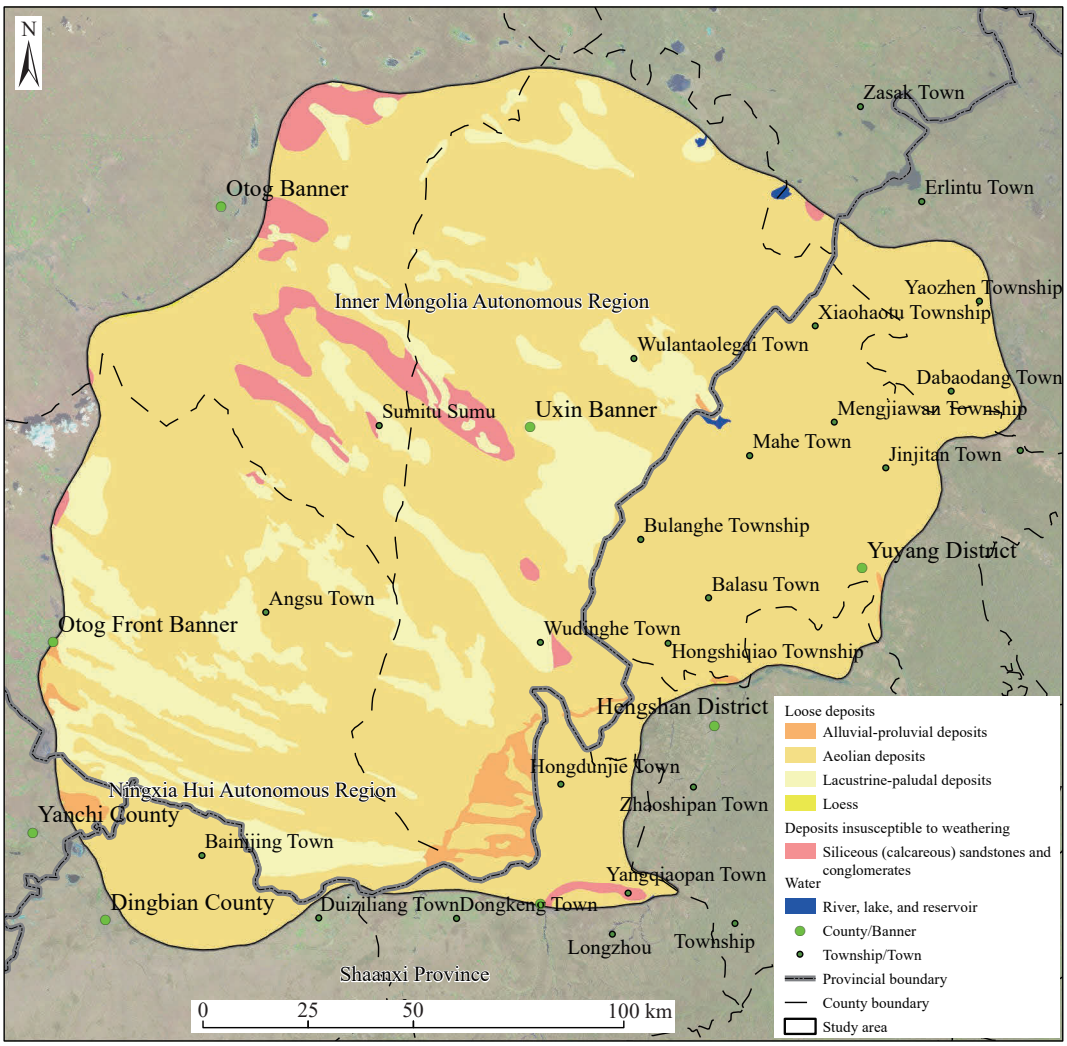

Fig. 2. Soil parent material type map of the study area.

2.4. Climate

The Mu Us Sandy Land, lying in the transitional zone between semi-arid and arid climates, has a typical temperate continental monsoon climate. The southeastern part of the study area has higher annual average precipitation and temperature compared to the northwestern part (Fig. 3). Over the past 20 years, the climate has shown a trend towards being warm and humid. The annual average temperature has slightly increased from 8.71°C during 2001–2005 to 9.12°C during 2016–2020. Annual precipitation has gradually increased with fluctuations, ranging from a minimum of 203.22 mm in 2005 to a maximum of 464.64 mm in 2017 (Table 3). Precipitation is mostly concentrated from July to September, accounting for over 60% of the total annual precipitation. Winter and spring experience strong and frequent winds, with average wind speeds ranging from 3.0–3.9 m/s in spring (Lu HY et al., 2005).

2.5. Hydrogeology

The Mu Us Sandy Land boasts abundant surface water and groundwater resources. Numerous rivers and lakes in the sandy land serve as the sources of surface water. With surface runoff up to 1.4×10^9 m^3, the surface water can be divided into endorheic and exorheic systems. The endorheic system is distributed in the northwestern and west-central parts of the sandy land, with an average multiyear runoff of inland rivers of about 1.05×10^8 m^3 (Yu N, 2018). The lakes in this system are mainly saline alkaline lakes, with freshwater lakes found

Table 1. Types and areas of soil parent materials in the study area.

Type	Category	Area/km^2	Percentage
Loose deposits	Alluvial and proluvial deposits	459.25	1.40%
	Aeolian sands	26378.39	80.33%
	Lacustrine and paludal deposits	4874.55	14.84%
	Loess	14.03	0.04%
Sediments insusceptible to weathering	Siliceous (calcareous) sandstones and conglomerates	1074.39	3.27%
Water	Water	38.73	0.12%
Total		32839.34	100%

Table 2. Characteristics of vegetation formations in the study area (after Bai GS et al., 2006).

Group	Distribution	Primary formations
Steppes and shrubs	Tablelands in Otog Banner in the west, and low and gentle tablelands in Dingbian, Yanchi, and Otog Front Banner in the southwest	Form. *Stipa bungeana* + *Lespeza dahurica*, Form. *Stipa gobica* + *Artimisia frigida*, and Form. *Artemisia frigida*
Psammophytic vegetation	Predominant vegetation with the broadest distribution area in the Mu Us Sandy Land	Form. *Artemisia ordosica*, Form. *Artemisia sphaerocephala*, Form. *Psammochloa villosa*, and Form. *Caragana korshinskii*
Meadows, and halophilic and swamp vegetation	Most extensive azonal vegetation distributed in depressions and river valleys in the Mu Us Sandy Land	Form. *Puccinellia tenuifolla*, Form. *Achnatherum splendens*, Form. *Iris ensata*, Form. *Suaeda corniculate*, S. *heteroptera*, Form. *Kalidium cuspidatum*, *K. foliatum*, and Form. *Phragmites communis*

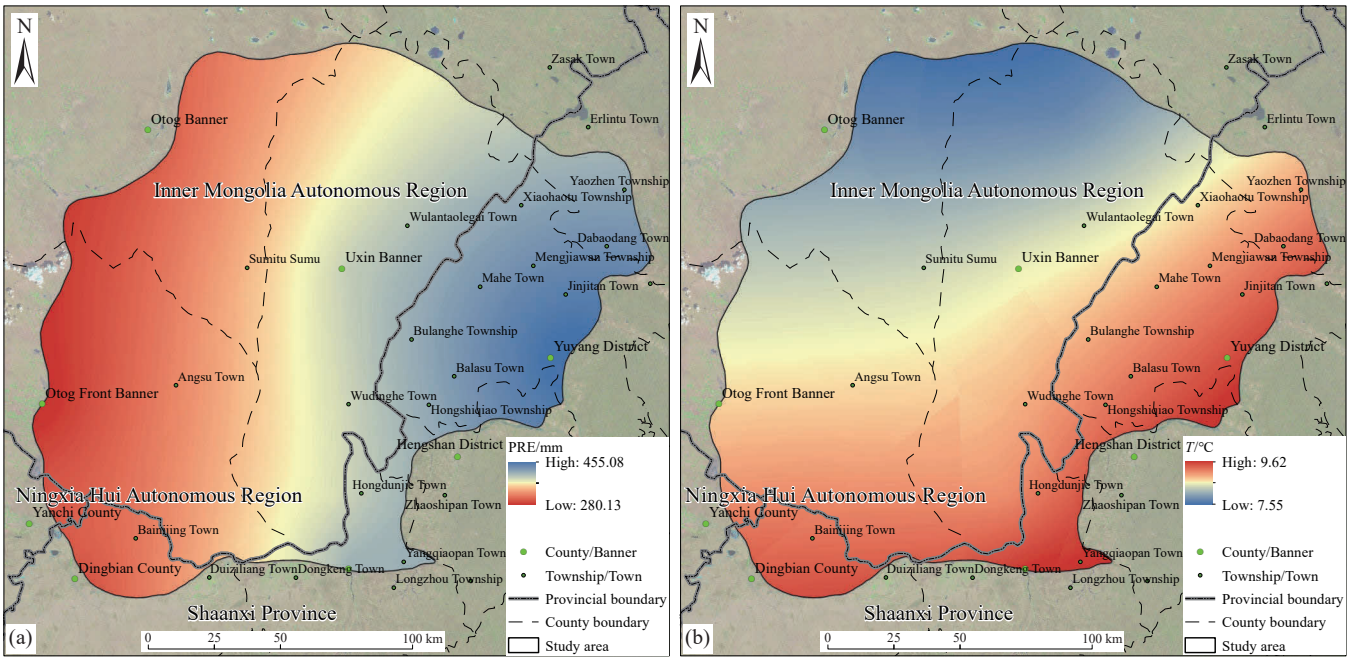

Fig. 3. a–Average precipitation map; b–average temperature map of the study area from 2001 to 2020.

Table 3. Statistics of annual average temperatures and annual precipitation in the study area during 2001–2020 (annual average temperature: °C; annual precipitation: mm).

Year	Uxin Banner station		Yulin station		Hengshan station		Jingbian station		Henan station		Wushenzhao station		Dingbian station		Yanchi station		Otog Front Banner station		Otog Banner station	
	Annual average temperature	Annual precipi-tation	Annual average temperature	Annual precipi-tation	Annual average temper-ature	Annual precipi-tation	Annual average tempera-ture	Annual precipita-tion	Annual average temper-ature	Annual precipi-tation	Annual average tempera-ture	Annual precipi-tation	Annual average tempe-rature	Annual precipi-tation	Annual average temper-ature	Annual precipi-tation	Annual average tempera-ture	Annual precipi-tation	Annual average temper-ature	Annual precip-itation
2001	8.57	422.40	9.78	568.70	9.95	426.00	9.66	474.20	8.30	427.60	7.54	302.00	9.55	504.90	9.52	387.70	8.69	298.40	8.42	269.40
2002	8.77	613.60	9.78	526.60	9.78	483.00	9.87	546.30	8.17	544.10	7.47	429.20	9.79	361.10	9.79	399.10	8.69	342.30	8.43	355.50
2003	8.01	381.10	9.17	436.30	9.14	406.30	9.28	462.70	7.94	319.70	6.90	379.70	8.99	341.40	8.20	293.90	8.21	235.30	7.86	352.60
2004	8.53	401.40	9.58	420.00	9.83	300.90	9.79	250.50	8.13	292.10	7.28	357.80	9.52	320.00	8.27	262.00	8.44	228.20	8.03	290.80
2005	8.27	178.40	9.14	248.70	9.43	267.40	9.40	300.60	7.72	204.00	6.67	164.60	9.18	233.80	8.07	180.00	8.10	118.80	7.80	135.90
2006	9.12	320.30	10.11	313.50	10.35	272.80	10.49	216.70	8.92	162.90	7.67	323.30	10.18	268.10	9.20	212.10	9.17	191.90	8.57	256.70
2007	8.99	485.50	9.80	439.40	9.74	416.40	10.01	477.30	8.33	347.70	7.44	428.40	9.62	448.90	8.73	284.10	8.56	314.10	8.29	316.50
2008	8.29	316.50	8.95	447.50	9.05	433.90	9.16	444.90	7.43	242.50	6.55	409.20	8.98	251.20	8.00	266.70	7.94	301.20	7.62	297.90
2009	8.87	341.90	9.54	420.80	9.69	341.90	9.31	367.30	8.22	296.20	7.16	262.60	9.60	348.00	8.69	280.70	8.76	247.80	8.22	207.20
2010	8.58	310.30	9.40	363.90	9.52	361.20	9.57	354.60	8.34	315.40	7.14	302.60	9.53	328.50	8.87	248.40	8.83	250.40	7.90	311.10
2011	8.01	367.30	8.79	445.40	8.69	464.60	8.77	458.20	7.52	616.10	6.63	277.60	8.69	418.80	8.19	402.80	7.88	454.00	7.64	191.40
2012	7.93	604.10	8.56	566.80	8.42	498.90	8.52	462.20	7.23	484.70	6.24	380.80	8.74	427.60	8.19	308.00	7.81	319.20	6.63	318.50
2013	9.61	370.90	10.06	562.50	9.85	398.20	10.08	443.50	8.49	383.40	7.76	403.60	10.34	329.10	9.56	288.20	9.38	266.00	7.93	207.00
2014	9.25	337.90	10.05	378.30	9.75	310.10	10.06	473.70	8.16	363.70	7.52	432.20	9.89	453.10	9.38	346.90	8.87	260.20	7.93	213.00
2015	9.38	419.40	10.15	451.00	10.21	378.10	10.46	359.90	8.54	338.40	7.77	335.20	10.16	383.80	9.54	365.60	9.08	269.10	8.10	251.70
2016	9.19	457.70	9.82	724.90	9.99	506.00	10.39	405.60	8.60	415.10	7.55	568.00	10.28	317.10	9.54	347.70	9.13	269.70	7.65	349.80
2017	9.53	426.80	9.86	639.30	9.91	614.50	10.33	633.20	8.46	508.50	7.85	386.60	10.16	438.20	9.54	393.30	9.29	286.60	7.98	319.40
2018	9.09	494.00	9.61	696.70	9.72	519.20	10.11	445.30	8.40	386.40	7.36	516.80	9.99	430.70	9.45	385.50	9.04	259.10	7.63	467.90
2019	9.46	353.40	10.12	525.50	9.99	429.30	10.36	389.70	8.51	401.00	7.58	369.20	10.09	381.70	9.43	323.20	9.10	321.40	7.79	290.10
2020	9.05	282.20	9.60	346.30	9.60	313.90	9.91	426.90	7.79	333.70	7.05	345.60	9.74	304.40	9.07	205.80	8.68	206.30	7.52	339.40

in depressions between sand dunes. The exorheic system spreads across the southeastern part of the Mu Us Sandy Land and is part of the Yellow River system. It consists mainly of the Tuwei, Wuding, and Kuye rivers. The Ordos Platform, where the Mu Us Sandy Land is located, is a vast groundwater basin (He TH, 2009). The shallow groundwater resources in this area, located approximately 70 m below the Ordos Platform, are estimated to reach 2.2×10^9 m^3. The allowable withdrawal of groundwater is approximately 1.3×10^9 m^3 (Li C, 2019). The depth of burial of shallow groundwater in the Mu Us Sandy Land is usually less than 2.5 m in interdunal depressions and sometimes as shallow as 0.5 m in certain areas. In contrast, the groundwater in the southeast generally has deep burial depths, mostly exceeding 10 m (Fig. 4). The Mu Us Sandy Land primarily recharges its groundwater through meteoric water, resulting in satisfactory water quality across most areas of the sandy land, with a total dissolved solids (TDS) concentration lower than 1 g/L. In comparison to other deserts in China, the Mu Us Sandy Land has richer water resources and more favorable water conditions (Mao L, 2019).

2.6. Soils

The Mu Us Sandy Land is characterized by the prevalence of aeolian sandy soils. However, due to variations in soil moisture and vegetation types across fixed, semi-fixed, and shifting sandy land and interdunal depressions, a diverse range of soil types can be observed in the study area. Zonal soil characteristics are observed in the well-developed soils of fixed dunes, which are primarily composed of chestnut soils. These soils are mainly present in the tablelands and cover approximately 1517.51 km^2 or 4.62% of the total study area. Azonal aeolian sandy soils are the most widely distributed soil type in the sandy land and are found in semi-fixed and shifting sandy land across 77.27% of the study area. Fluvo-aquic soils (4169.23 km^2), swampy soils (402.76 km^2), and meadow solonchaks (273.87 km^2) are frequently found in interdunal depressions (Fig. 5; Table 4). The soils in the study area generally show low nutrient content, loose structures, and low moisture and fertility preservation capacities, making them prone to sand blows.

3. Methodology

3.1. Assessment index system

This study established a scientific index system by referencing existing studies on ecological vulnerability assessment (Shao HY et al., 2016; He L et al., 2018; Zang Z

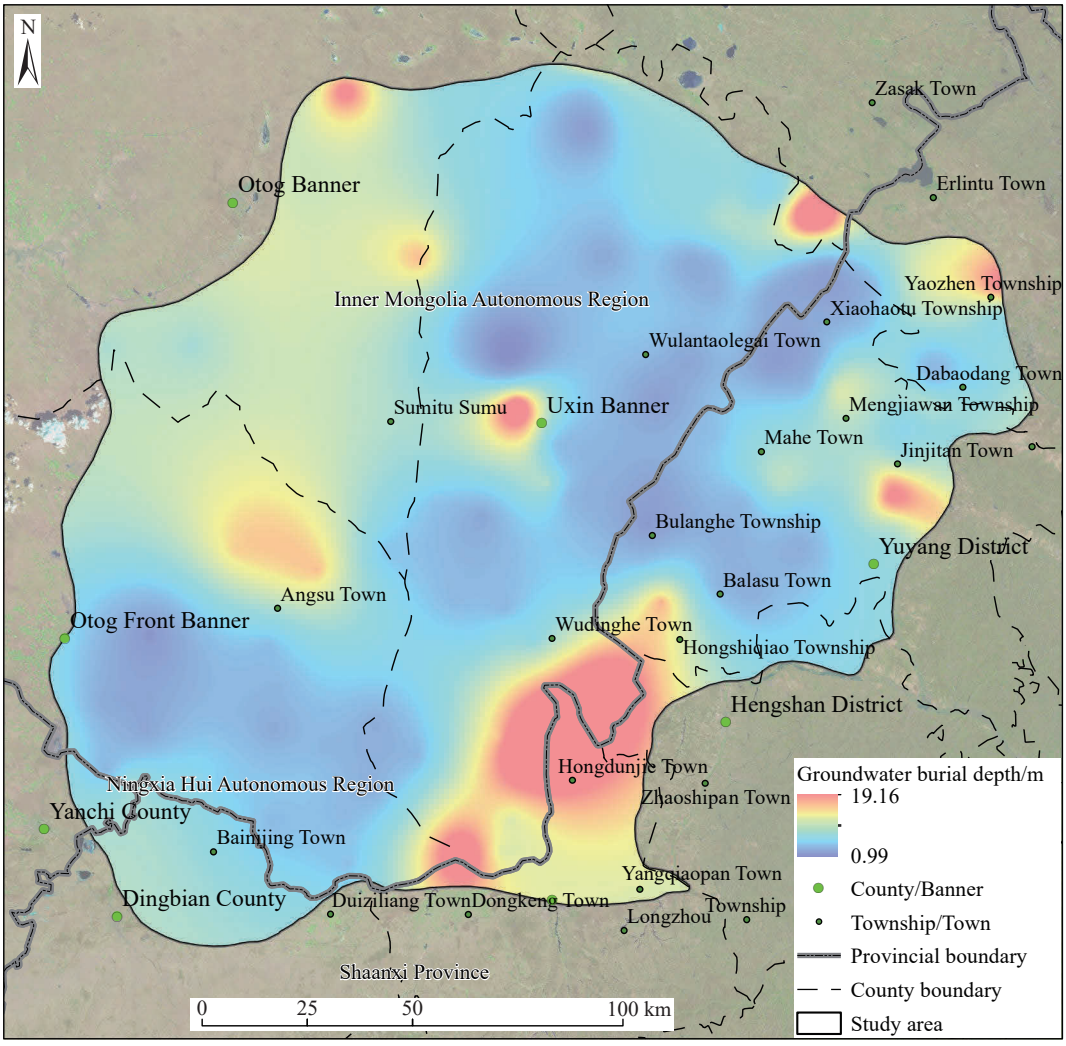

Fig. 4. Map showing the groundwater burial depths in the study area.

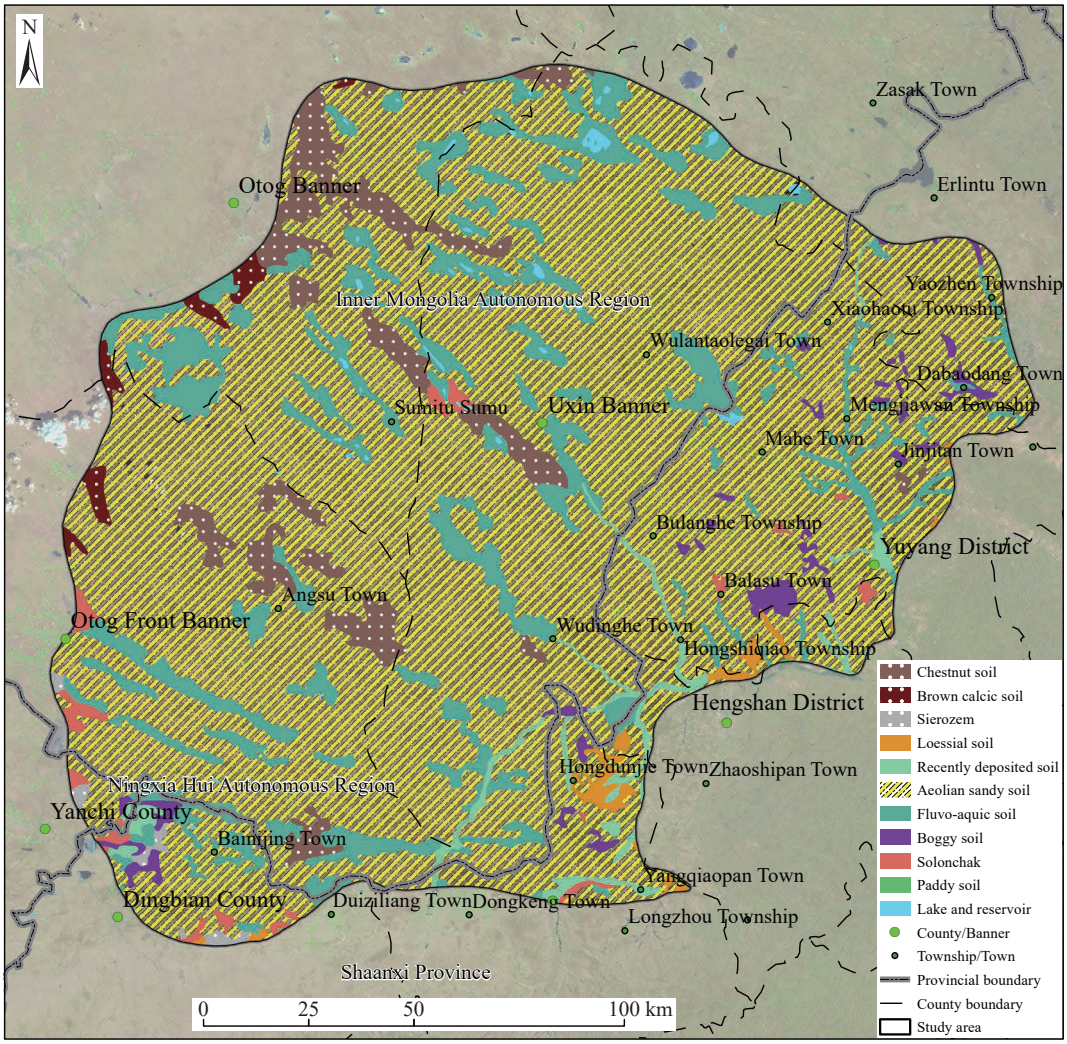

Fig. 5. Map showing the soil types in the study area.

Table 4. Types and areas of soils in the study area.

Type	Area/km^2	Proportion in the total study area
Meadow solonchak	273.87	0.83%
Fluvo-aquic soil	4169.23	12.70%
Aeolian sandy soil	25376.37	77.27%
Loessal soil	225.26	0.69%
Sierozem	89.63	0.27%
Chestnut soil	1517.51	4.62%
Paddy soil	2.17	0.01%
Recently deposited soil	526.59	1.60%
Swampy soil	402.76	1.23%
Brown calcic soil	217.20	0.66%
Water	38.73	0.12%
Total	32839.34	100%

et al., 2017) and following eco-geological research philosophy and the principles of comprehensiveness, predominance, scientificity, and operability. The index system included 15 factors grouped into five categories: Geology, meteorology, soil, landform, and vegetation (Table 5).

3.1.1. Principles of assessment index selection

Comprehensiveness: The study area spans about 260 km from east to west and around 210 km from north to south, thus exhibiting significantly different factors such as climates, geology, landforms, and groundwater. Therefore, the assessment indices should comprehensively reflect the diverse eco-geological conditions of the entire study area.

Predominance: The study area features highly heterogeneous landscapes, transitioning from a temperate monsoon climate to a temperate continental climate, and from desert steppe to loess hills and shrub steppes. It suffers significant wind erosion and severe sandy desertification. Hence, the assessment indices should be representative of the eco-geological characteristics of the study area.

Scientificity: The eco-geological vulnerability assessment aims to evaluate the eco-geological conditions of the study area by considering multiple factors, including geology, geomorphology, soil, and meteorology. Consequently, the assessment index system should be scientifically established by incorporating relevant research findings and referencing existing assessment systems.

Operability: The eco-geological vulnerability assessment should be conducted based on the combination of the regional characteristics of the study area with the microscopic data obtained from field surveys. Furthermore, both quantitative

Table 5. Index system for the eco-geological vulnerability assessment of the Mu Us Sandy Land.

Criterion layer	Index layer	Factor layer	AHP-derived weight	Weight derived using the EWM	Comprehensive weight
Eco-geological vulnerability of the Mu Us Sandy Land	Meteorology	Air temperature (–)	0.0623	0.0498	0.0475
		Precipitation (–)	0.0601	0.1985	0.1824
		Wind speed (+)	0.0634	0.0271	0.0263
		Evapotranspiration (+)	0.0580	0.1053	0.0935
	Landform	Slope (+)	0.0806	0.0404	0.0498
		Aspect	0.0973	0.0404	0.0602
	Geology	Soil parent materials	0.0651	0.0441	0.0439
		Groundwater burial depth (+)	0.0697	0.1322	0.1410
	Soil	Fractal dimension (–)	0.0631	0.0269	0.0260
		N (–)	0.0594	0.0611	0.0556
		P (–)	0.0601	0.0611	0.0562
		K (–)	0.0674	0.0611	0.0630
		Organic matter (–)	0.0597	0.0101	0.0092
	Vegetation	Type	0.0752	0.0709	0.0818
		Vegetation Cover (–)	0.0586	0.0710	0.0636

Notes: (1) The fractal dimension of soil, a parameter describing the geometric shape of soil particles, can reveal the changing patterns of soil textures. A finer soil texture corresponds to a higher fractal dimension, and vice versa (Zhang JR et al., 2004). The method for calculating fractal dimension is shown in Yan X et al., 2017. (2) (+) and (–) represent positive and negative indices, respectively.

and qualitative data should be effectively utilized. Therefore, it is necessary to consider the operability of data acquisition.

3.1.2. Basis for assessment index selection

Meteorology: From east to west, the study area shifts from a desert steppe to a steppe desert, with annual average precipitation decreasing and annual average temperature increasing. The distribution of community types in the study area is influenced by both heat and water. Additionally, the intensity of wind erosion can be inferred by measuring wind speed. Therefore, the precipitation, temperature, and wind speed were selected as assessment indices in this study.

Vegetation: The vegetation cover is a comprehensive quantitative measure that represents the extent of surface covered by vegetation communities. It is an important parameter for describing vegetation communities and ecosystems. As the study area exhibits significant changes in the spatial distribution of vegetation, differences in eco-geological conditions among regions can be reflected by variations in vegetation types and vegetation cover. Therefore, the vegetation cover and vegetation type were selected as assessment indices in this study.

Soil: Organic matter is an essential energy source for both animals and plants, and it plays a key role in improving soil structures. Total nitrogen is a crucial element for the growth and development of plants, directly influencing plant growth. Total nitrogen also plays a vital role in regulating the structure and function of the ecological environment, as well as the primary and secondary productivity of vegetation communities in grassland ecosystems (Luo RY et al., 2015). Phosphorus and potassium are essential nutrients for plant growth and development. The fractal dimension can reflect the changes in soil structures (Tyler SW et al., 1992). Therefore, fractal dimension and the contents of organic matter, total nitrogen, total phosphorus, and total potassium were selected as assessment indices in the study area.

Geology: Soil parent materials, resulting from rock weathering, provide a material basis for soil formation. Diverse soil parent materials influence the properties of their overlying soils to some extent. Studies have shown that different soil parent materials can significantly affect site conditions such as exchangeable calcium, total nitrogen, soil depth, and the N, P, Ca, K, and Mg contents in leaves, while the differences in geochemistry, fracture development, and weathering-induced nutrients between different soil parent materials also have significant effects on vegetation growth (Eimil-Fraga C et al., 2014; Hahm WJ et al., 2014; Jiang ZH et al., 2020). The vegetation distribution in the study area shows zonal characteristics with an increase in groundwater burial depth. The aquatic vegetation zone, transitional zone, and xeromorphic vegetation zone can be identified from the margin of interdunal wetland to sand dunes or sandy land. The plants in the aquatic vegetation zone include *Carex*, *Achnatherum splendens*, and *Phragmites australis*, the plants in the transitional zone are dominated by *Cynanchum komarovii*, *Caragana korshinskii*, *Artemisia sphaerocephala*, *Phragmites australis*, and *Salix psammophila*, and the plants in the xeromorphic vegetation zone consist of *Artemisia sphaerocephala* and *Caragana korshinskii* (Cheng DH et al., 2012). Therefore, soil parent materials and the groundwater burial depth serve as an assessment index.

Landform: The Local microclimatic characteristics are dictated by elevation, slope, and aspect, which can influence the vegetation cover and distribution of vegetation types. Although the study area is high in the northwest and low in the southeast, this area exhibits relatively small height differences overall and insignificant vertical zonation of vegetation cover. Field surveys reveal that vegetation grows better in gentle zones than in steep slope zones, and windward slopes of sand dunes show significantly lower vegetation cover than their leeward slopes. Therefore, the slope and aspect were selected as assessment indices.

3.2. Data sources

The data used in this study included meteorological data, DEM data, types of soil parent materials, groundwater burial depths, vegetation cover, vegetation types, and the contents of nitrogen, phosphorus, potassium, and organic matter in soils. Among them, the meteorological data (2001–2020) and DEM data (resolution: 30 m) were sourced from the Resource and Environment Science and Data Center (https://www.resdc.cn/) and the Geospatial Data Cloud (http://www.gscloud.cn/), respectively. Information on soil parent materials was collected through eco-geological surveys (to be published). The groundwater burial depths were obtained through field monitoring conducted in June 2020. Soil samples were also collected and analyzed for total nitrogen, total phosphorus, total potassium, organic matter content, and soil texture. Land use data were determined through the interpretation of Landsat-8 remote sensing images obtained in the summer of 2020, with the land use classification standard aligning with that of the 3rd National Land Resource Survey. The vegetation types can be found in the *Vegetation Map of The People's Republic of China* (1∶1000000) (Zhang XS, 2007).

In this study, the dimidiate pixel model was employed to calculate the fractional vegetation cover (*FVC*) using the following equation (Equ. 1; Yang SW et al., 2015):

$$FVC = \frac{NDVI - NDVI_{soil}}{NDVI_{veg} - NDVI_{soil}} \quad (1)$$

where *NDVI* is the normalized difference vegetation index, and $NDVI_{soil}$ and $NDVI_{veg}$ are *NDVI* values of the surfaces without vegetation cover and completely covered by vegetation, respectively.

The modified Penman-Monteith equation recommended by FAO was used to calculate the potential evapotranspiration (E_0, Equ. 2; Allen RG et al., 1998):

$$E_0 = \frac{0.408\Delta(R_n - G) + \frac{900}{T+273}\gamma u_2(e_s - e_a)}{\Delta + \gamma(1 + 0.34u_2)} \quad (2)$$

where Δ is the slope of the saturation vapor pressure *vs.* temperature curve, kPa/°C; R_n is the net radiation, MJ/(m^2·d); G is the surface heat flux, MJ/(m^2·d); T is the average temperature, °C; γ is the hygrometer constant, kPa/°C; u_2 is the wind speed at 2 m, m/s; e_s is the saturation vapor pressure, kPa, and e_a is the actual vapor pressure, kPa.

Since R_n data are unavailable in most observation stations, R_n was calculated based on the sunshine duration N. u_2 was converted from the wind speed at 10 m above the ground, and the slope of the saturation vapor pressure *vs.* temperature curve was derived from the average temperature.

3.3. Sampling and testing

The vast study area exhibits significantly different natural conditions from the east to the west. To ensure an objective assessment, the sampling points in this study were arranged following the principles of uniformity, typicality, and accessibility. In other words, the sampling points should be distributed as evenly as possible in the study area and be representative within a certain range. Since the roots of *Artemisia sphaerocephala* and *Salix psammophila*, the most widespread vegetation in the study area, are well-developed in the soil layer at depths of 20–30 cm (Zhao L et al., 2012; Zhao M et al., 2018), soil samples in this study were primarily collected from the soil layer at the above depths. At each sampling point, three sub-samples with equal weights were taken from the same depth and then mixed into one test sample. Each test sample, for which impurities such as plant roots and gravels were removed, was placed in a clean plastic bag and numbered. Besides, each test sample weighed no less than 1 kg.

The mechanical composition of soil samples was tested using a laser particle size analyzer Mastersizer 3000 (Liu JY et al., 2024). The contents of total phosphorus and total potassium were determined using X-ray fluorescence spectrometry (XRF). The contents of total nitrogen and organic matter were determined using the semi-micro Kjeldahl method and the potassium dichromate volumetric method, respectively. To ensure the accuracy and precision of the analysis, the sample analysis process followed the *Specification of Land Quality Geochemical Assessment* (DZ/T 0295201). The accuracy and precision of the analysis method were controlled using the national primary certified reference materials (GBW series). Furthermore, the recovery of various indices was within the allowable range of the national certified reference materials. The sample test results are detailed in Appendix Table 1.

3.4. Evaluation methods

3.4.1. Data pre-processing

The spatial interpolation method can predict the values of unknown points based on the values of known points to form a smooth surface, thus achieving the expansion from points to a surface. Hence, it can effectively simulate the spatial distributions of assessment factors, such as precipitation, air temperature, and soils' physical and chemical parameters. This study employed the empirical Bayesian Kriging (EBK) method in ArcGIS 10.6 for the interpolation of 9 factors including air temperature, precipitation, and wind speed. However, soil parent materials serve as a descriptive factor, and the effects of the aspect on eco-geological vulnerability do not increase linearly with the slope gradient. Given this, the classification and assignment criteria for soil parent materials, aspect, and vegetation type were formulated (Table 6) by integrating other researchers' study results and the specific conditions of the Mu Us Sandy Land (Zhang XS et al., 2017a; Hong WY et al., 2016; Zhang JH et al., 2021b). To ensure consistency in spatial analysis, all the data were converted into Gauss Kruger projections, 30-m-resolution raster images (Fig. 6).

3.4.2. Data normalization

In this study, the range method was used to normalize

various data and remove dimensions. The assessment indices were divided into positive and negative indices, based on the relationships between factors and eco-geological vulnerability. Positive indices are those that positively correlate with eco-geological vulnerability, while negative indices do not. A higher positive index value suggests higher

Table 6. Grading and values of soil parent materials and aspect of the study area.

Value	1	3	5	7	9
Soil parent materials	Aeolian sandy sediments		Siliceous (calcareous) sandstones and conglomerates, loess, and water bodies	Alluvial-proluvial deposits	Lacustrine-paludal deposits
Aspect	315°–0°	0°–45° 270°–315°	225°–270°	45°–90° 180°–225°	−1° 90°–135° 135°–180°
Vegetation type	Subshrub - low subshrub desert, succulent halophytic low-subshrub desert, and shrub desert	Temperate short bunchgrass - short subshrub the desert steppe, and temperate bunchgrass steppe	Dogstail - carex - broad-leaved herb swamp meadow, dogstail - broad-leaved herb meadow, dogstail - broad-leaved herb salt meadow, annual grain crop - cold-resistant cash crop field, and water bodies	Temperate deciduous shrubs	Temperate broad-leaved deciduous forest

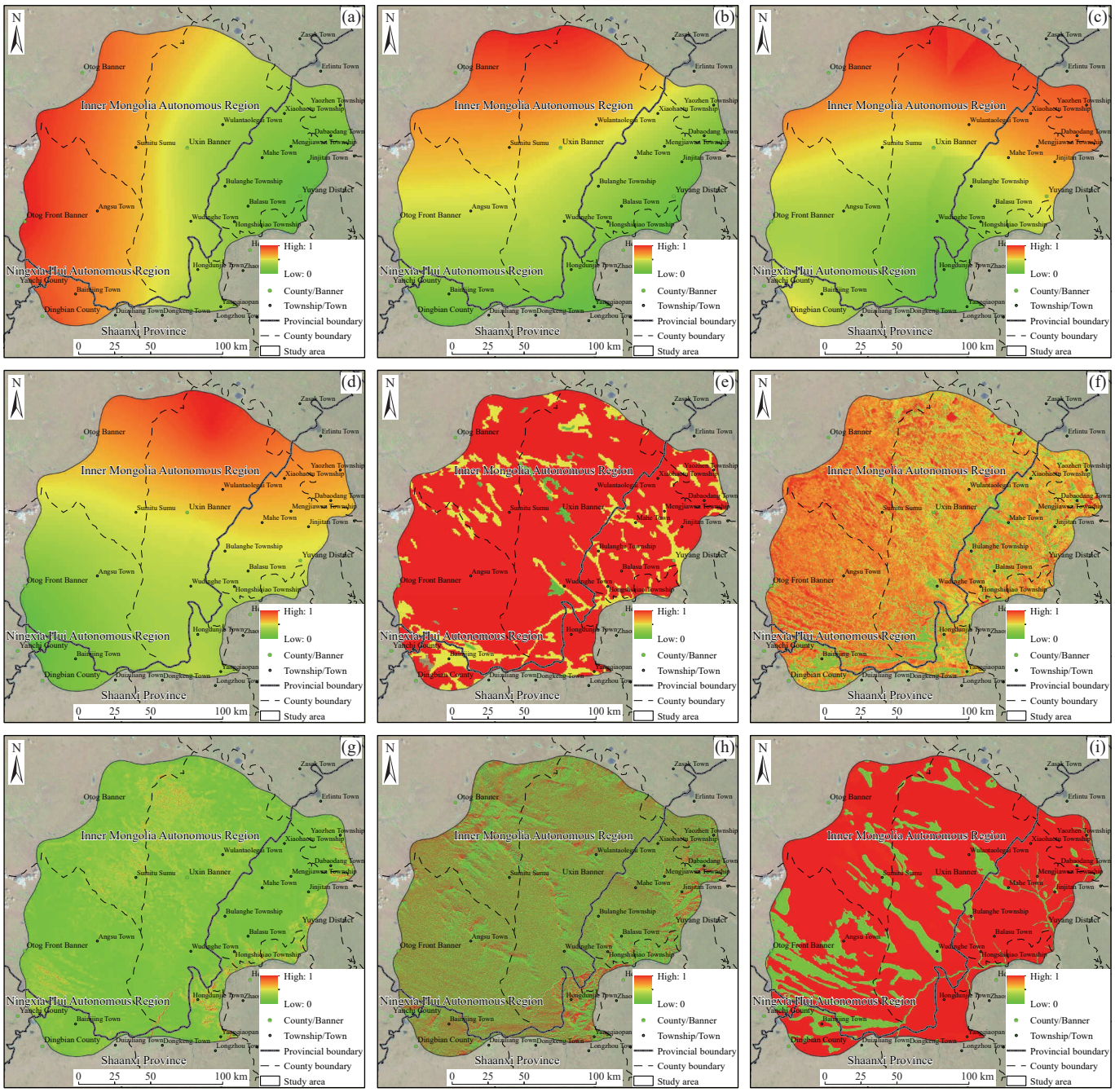

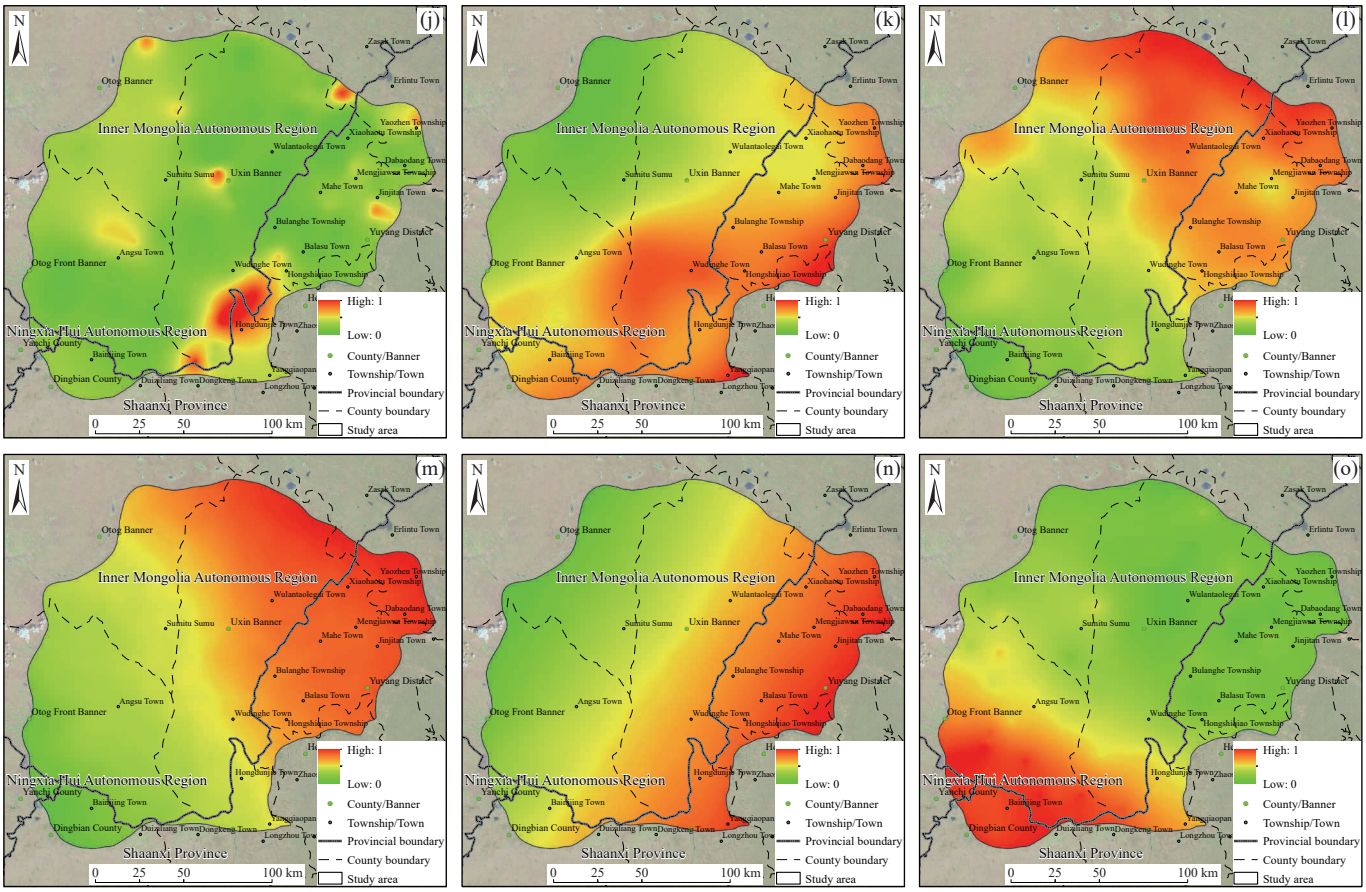

Fig. 6. Interpolation (values assigned) results of all assessment indices in the study area. a–average precipitation; b–average temperature; c–average wind speed; d–average evapotranspiration; e–vegetation type; f–vegetation cover; g–slope; h–aspect; i–soil parent materials; j–groundwater burial depth; k–fractal dimension of soil; l–organic matter; m–total nitrogen; n–total phosphorus; o–total potassium.

eco-geological vulnerability. The calculation equations are as follows (Equs. 3, 4):

$$\text{Positive index} \quad X_i' = \frac{X_i - X_{min}}{X_{max} - X_{min}} \tag{3}$$

$$\text{Negative index} \quad X_i' = \frac{X_{max} - X_i}{X_{max} - X_{min}} \tag{4}$$

3.4.3. AHP

The AHP, a multi-criteria decision-making method, has been adopted in almost all decision-related applications (Vaidya OS et al., 2006; Hu XJ et al., 2021; Wang KF et al., 2014). It can decompose a complex system problem into multiple elements. Then, according to the mutual relationships between elements, it can divide the elements into several levels, including the goal, criterion, and index layers (Table 5). The calculation steps include constructing judgment matrices, calculating index weight vectors, and conducting a consistency check of results. The construction of judgment matrices is a crucial step in the AHP method. Generally, after pairwise comparison of factors, values of 1 to 9 are assigned to the factors to indicate their importance, with 9 representing the most important factor and 1 the least important. In this study, the judgment matrices for eco-geological vulnerability factors in the Mu Us Sandy Land were constructed based on existing research results and field survey findings, as shown in Table 5. The consistency check of the judgment matrices yielded a random consistency ratio (CR) less than 0.1, suggesting that the constructed judgment matrices exhibited qualified random consistency and were rational. The weights of the assessment factors are listed in Table 7.

3.4.4. Entropy weight method

The EWM is a data-driven, objective weighting method based on information theory. By calculating the information entropy of indices, this method can measure the effective information and index weights contained in known data based on the differences of indices. Lower information entropy suggests more stable and reliable data and higher index weights. Otherwise, higher information index weights correspond to lower index weights. The calculation method is as follows (Wang Q et al., 2017):

For n samples and m indices, according to the definition of entropy, the entropy H_i of the ith index is (Equ. 5):

$$H_i = -k\sum_{j=1}^{n}\left(f_{ij} ln f_{ij}\right) \tag{5}$$

where $f_{ij} = \frac{R_{ij}}{\sum_{j=1}^{n} R_{ij}}$, and k is the adjustment coefficient, $k = \frac{1}{\ln n}$. If $f_{ij} = 0$, then $f_{ij} ln f_{ij} = 0$. The weight of the ith index is (Equ. 6):

Table 7. Judgement matrices for eco-geological vulnerability assessment of the Mu Us Sandy Land.

a. Judgement matrix for the index layer

Decision objective	Meteorology	Geology	Landform	Vegetation	Soil	Consistency check
Meteorology	1	2	4	3	2	λ_{max}=5.0524
Geology	−	1	2	1	1	*CI*=0.0131
Landform	−	−	1	0.50	1/3	*RI*=1.12
Vegetation	−	−	−	1	0.50	*CR*=0.0117
Soil	−	−	−	−	1	

b. Judgement matrix for meteorological indices

Meteorology	Temperature	Precipitation	Wind speed	Consistency check
Temperature	1	0.3333	3	λ_{max}=1.1327
Precipitation	−	1	5	*CI*=0.0442
Wind speed	−		1	*RI*=0.90
Evapotranspiration				*CR*=0.0491

c. Judgement matrix for geological indices

Geology	Soil parent materials	Groundwater burial depth	Consistency check
Soil parent materials	1	0.5	λ_{max}=2.0000
Groundwater burial depth	−	1	*CI*=0
			RI=0, *CR*=0

d. Judgement matrix for landform indices

Topography	Slope	Aspect	Consistency check
Slope	1	1	λ_{max}=2.0000
Aspect	−	1	*CI*=0
			RI=0, *CR*=0

e. Judgement matrix for vegetation indices

Vegetation	Vegetation type	Vegetation cover	Consistency check
Vegetation type	1	1	λ_{max}=2.0000
Vegetation cover	−	1	*CI*=0
			RI=0, *CR*=0

f. Judgement matrix for soil indices

Soil	N	P	K	Organic matter	Fractal dimension	Consistency check
N	1	1	1	3	5	λ_{max}=5.1508
P	−	1	1	3	5	*CI*=0.0337
K	−	−	1	3	5	*RI*=1.12
Organic matter	−	−	−	1	5	*CR*=0.0337
Fractal dimension	−	−	−	−	1	

$$W_i = \frac{1 - H_i}{m - \sum_{i=1}^{m} H_i} \quad (6)$$

where f_{ij} is an element in the normalized matrix, H_i is the entropy of the ith index, and W_i is the weight of the ith index.

3.4.5. Calculation of comprehensive weights

Since the index selection, weight assignment, and vulnerability classification in the AHP are somewhat subjective, the AHP-derived results may not objectively reflect the actual situation. Given this, this study integrated the results calculated using the EWM and AHP methods to acquire more scientific comprehensive weights, as calculated using the following equation (Equ. 7; Tan SJ, 2018):

$$W_j = \frac{W_j^1 \times W_j^2}{\sum_{j=1}^{n} W_j^1 \times W_j^2} \quad (7)$$

where W_j is the comprehensive weight of the jth factor, and W_j^1 and W_j^2 are the weight results calculated using the AHP and the EWM, respectively. The comprehensive weights of all the indices are given in Table 5.

3.4.6. EGVI

The EGVI was calculated using the weighted linear combination method, and the calculation equation is as follows (Equ. 8):

$$EGVI_i = \sum_{i=1}^{n} M_{ij} \times W_j \quad (8)$$

where $EGVI_i$ is the EGVI of the ith unit; n is the total number of factors; W_j is the weight of the jth factor, and M_{ij} is the value of the jth factor in the ith unit.

3.4.7. Spatial autocorrelation analysis

Spatial autocorrelation is a method to examine the dependency relationships and levels of a certain object or phenomenon by constructing statistics for a particular attribute or characteristic. This method enables the description of clustered or dispersed distributions of spatial object attributes. Spatial correlation includes positive and negative correlations. The former means that the attributes of adjacent spatial units show the same changing trend, while the latter means the opposite. Spatial autocorrelation can be divided into global and local spatial autocorrelations. Global spatial

autocorrelation is used to judge whether an attribute of the entire dataset exhibits spatial correlation or clustering, while local spatial autocorrelation is used to judge the local spatial clustering pattern (Hu XJ et al., 2021). Their equations are as follows (Equs. 9, 10):

$$\text{Global Moran's I index}: I = \frac{\sum_{i=1}^{n}\sum_{j=1}^{n} w_{ij}(x_i-\bar{x})(x_j-\bar{x})}{\sum_{i=1}^{n}\sum_{j=1}^{n} w_{ij}\sum_{i=1}^{n}(x_i-\bar{x})^2} \quad (9)$$

$$\text{Local Moran's I index}: I = \frac{(X_i-\bar{X})}{S^2}\sum_{j} W_{ij}(X_j-\bar{X}) \quad (10)$$

where I is the Moran's I index; Xi and Xj are the vulnerability index averages of the ith and jth grids, respectively; X is the vulnerability index average of all grids; Wij is the spatial weight matrix, and S is the sum of the elements in the spatial weight matrix.

Based on the calculation of the local Moran's I index, the study determined the local indicators of spatial association (LISA) cluster map through spatial clustering. Within a 95% confidence interval, the eco-geological vulnerability was further divided into five different types: High-high cluster zone (H-H), high-low outlier zone (H-L), low-high outlier zone (L-H), low-low cluster zone (L-L), and nonsignificant zone. The meanings of these types are shown in Table 8.

4. Results

At present, there is no standardized criterion for the evaluation of eco-geological vulnerability in a unified manner. Therefore, this paper has referred to the research method used for ecological vulnerability. Generally, the equisection method or the Natural Breaks is used to classify ecological vulnerability (Zhao JC et al., 2018; He L et al., 2018; Zhang F et al., 2017). The Natural Breaks is an efficient and accurate approach for objective data classification, which is commonly used in mathematical model calculations. This method can provide satisfactory classification results for continuous data. Its core principle is similar to that of the clustering method. In other words, the data within one group exhibit the maximum similarity, while the data between groups exhibit the maximum dissimilarity. Furthermore, the Natural Breaks tries to ensure similar ranges and numbers of elements for all groups. Considering the continuity of eco-geological vulnerability indices in the study area, the study classified the eco-geological vulnerability of the study area into five grades using the Natural Breaks (Fig. 7; Table 9). Overall, the study area presents increasingly severe eco-geological vulnerability from east to west. This area exhibits vulnerable eco-geological conditions. The extremely and highly vulnerable zones and the potentially and slightly vulnerable zones cover areas of 13069.00 km^2 and 10478.26 km^2, respectively, which account for 39.80% and 31.91% of the total study area.

The extremely vulnerable zones, which are distributed in the northern and southeastern parts of the study area, are situated primarily in the area from Angsu Town to Otog Front Banner, the northern Uxin Banner, and the surrounding areas of Hongdunjie Town. They cover an area of 4871.65 km^2, accounting for 14.83% of the study area. The area from Angsu Town to the Otog Front Banner features low annual average temperatures, high average wind speeds, and low precipitation. The extremely high eco-geological vulnerability of this area is primarily caused by extremely harsh meteorological conditions and aggravated by great landform fluctuations due to widespread mobile dunes. By contrast, the southeastern part shows much better meteorological conditions. However, this part is located in the transition zone between the sandy land and the Loess Plateau, with large landform fluctuations, higher fractal dimensions of soils, and groundwater burial depths greater than 10 m. Therefore, the southeastern part exhibits high eco-geological vulnerability.

The highly vulnerable zones are distributed in the western and southern parts of the study area. Surrounding the extremely vulnerable zones, these zones are primarily situated along the Angsu Town - Uxin Banner - Xiaohaotu Township area and the surrounding areas of Dingbian County. They cover a total area of 8197.35 km^2, which accounts for 24.96% of the study area. The high eco-geological vulnerability in the southwest mainly results from large groundwater burial depths and low annual average precipitation, followed by low total potassium content. By contrast, the high eco-geological vulnerability in the southeast is dominated by large groundwater burial depths, high fractal dimensions of soil, and low total phosphorus content.

The moderately vulnerable zones are distributed in the central and southwestern parts of the study area, especially in the central part. They act as transitional areas between the highly and extremely vulnerable zones and the potentially and slightly vulnerable zones. They cover an area of 9292.08 km^2, accounting for 28.30% of the study area. They show complex eco-geological conditions. For instance, these zones exhibit moderate total phosphorus content, the northern part of the study area shows high total nitrogen and organic matter contents but low total potassium content, while the southern part is opposite to the northern part. These zones exhibit relatively shallow groundwater burial depths, reducing the

Table 8. Meanings of different LISA clustering patterns.

Clustering type	Meaning
H-H	The region itself and its adjacent regions both exhibit relatively high eco-geological vulnerability, suggesting a convergent trend.
H-L	The region itself and its adjacent regions exhibit high and low eco-geological vulnerability, respectively, suggesting a divergent trend.
L-H	The region itself and its adjacent regions exhibit low and high eco-geological vulnerability, respectively, suggesting a divergent trend.
L-L	The region itself and its adjacent regions both exhibit relatively low eco-geological vulnerability, suggesting a convergent trend.
Nonsignificant	No significant spatial clustering

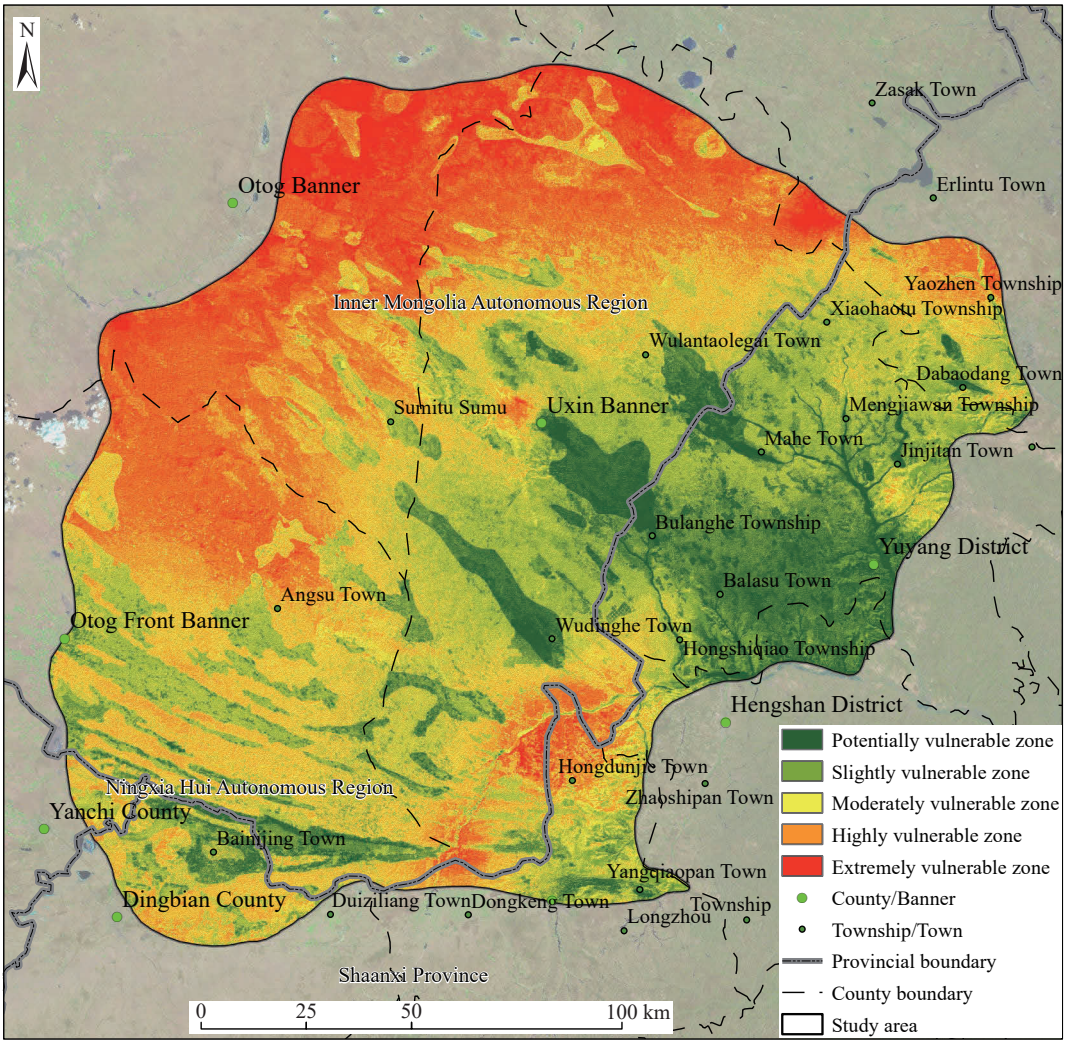

Fig. 7. Map showing the assessment results of eco-geological vulnerability in the study area.

impact of negative soils and meteorological conditions. Moreover, the soil parent materials originating from the lake-swamp deposits are distributed among sand dunes, playing a significant role in reducing local eco-geological vulnerability.

The potentially and slightly vulnerable zones are distributed in the eastern part of the study area. They cover areas of 7228.66 km^2 and 3249.60 km^2, respectively, which account for 22.01% and 9.90% of the total study area. Without clear boundaries between them, they are situated mainly in the Hongshiqiao Township - Dabaodang Town area and Baishijing Town. The eastern part exhibits high annual average temperatures, high precipitation, and low average wind speeds. Moreover, groundwater in the eastern part demonstrates shallow burial depths and high total potassium content. All the above advantages offset the effects of soils, such as low organic matter content, low total nitrogen and potassium contents, and high fractal dimensions. In addition, Baishijing Town exhibits low evapotranspiration, high nitrogen, phosphorus, potassium contents, and favorable soil parent materials and vegetation types, thus diminishing the eco-geological vulnerability in the eastern part.

The Inner Mongolia Autonomous Region, with the largest area of 23544.90 km^2 in the study area, exhibits varying levels of eco-geological vulnerability. The moderately and highly vulnerable zones of Inner Mongolia cover similar areas of 6637.23 km^2 and 7088.60 km^2, respectively, which account for 28.19 % and 30.11 % of the autonomous region within the study area. In addition, the extremely and potentially vulnerable zones of Inner Mongolia have areas of 4695.30 km^2 (19.94% of the region in the study area) and merely 1260.38 km^2, respectively. Otog Banner, located in the northwestern part of the study area, suffers relatively high eco-geological vulnerability, with extremely and highly vulnerable zones occupying 45.65% and 36.39% of the banner within the study area, respectively. Otog Front Banner, which is located in the southwestern part of the study area, is dominated by moderately vulnerable zones, followed by highly vulnerable zones, occupying 35.25% and 33.04% of the banner within the study area, respectively. Lastly, Uxin Banner, situated in the central part of the study area, is dominated by moderately vulnerable zones, followed by highly vulnerable zones, which occupy 30.50% and 25.43% of the banner within the study area (Table 9).

Shaanxi Province covers an area of 9106.63 km^2 in the study area. Differing from Inner Mongolia, Shaanxi is dominated by slightly and potentially vulnerable zones, with

Table 9. Classification indices and areas of eco-geological vulnerability in the study area.

Province (autonomous region)	City	County (district or banner)	Potential vulnerable zone GEVI: 0.282–0.402		Slightly vulnerable zone GEVI: 0.402–0.446		Moderately vulnerable zone GEVI: 0.446–0.478		Highly vulnerable zone GEVI: 0.487–0.531		Extremely vulnerable zone GEVI: 0.531–0.656		Total
Inner Mongolia	Ordos	Otog Banner	10.77	0.21%	182.10	3.61%	712.45	14.14%	1834.06	36.39%	2300.58	45.65%	5039.95
		Otog Front Banner	291.80	4.10%	1293.22	18.19%	2506.28	35.25%	2349.18	33.04%	669.55	9.42%	7110.03
		Uxin Banner	957.81	8.56%	2388.05	21.34%	3413.37	30.50%	2845.87	25.43%	1586.98	14.18%	11192.08
		Ejin Horo Banner	0.00	0%	0.02	0.01%	5.13	2.53%	59.49	29.33%	138.20	68.14%	202.84
Subtotal			1260.38	5.35%	3863.39	16.41%	6637.23	28.19%	7088.60	30.11%	4695.30	19.94%	23544.90
Shaanxi	Yulin	Dingbian County	141.88	11.62%	328.05	26.86%	471.33	38.60%	271.74	22.25%	8.18	0.67%	1221.19
		Hengshan District	268.42	39.32%	236.78	34.68%	125.41	18.37%	49.21	7.21%	2.90	0.43%	682.72
		Jingbian County	63.23	5.55%	310.04	27.24%	415.55	36.51%	265.04	23.28%	84.39	7.41%	1138.25
		Shenmu CIty	47.13	3.91%	269.28	22.35%	459.29	38.12%	349.86	29.04%	79.28	6.58%	1204.84
		Yuyang District	1467.05	30.19%	2189.57	45.06%	1083.73	22.30%	119.26	2.45%	0.02	0.00%	4859.62
Subtotal			1987.71	21.83%	3333.73	36.61%	2555.32	28.06%	1055.10	11.59%	174.77	1.92%	9106.63
Ningxia	Wuzhong	Yanchi County	1.51	0.80%	31.54	16.79%	99.54	53.00%	53.64	28.56%	1.57	0.84%	187.81
Subtotal			1.51	0.80%	31.54	16.79%	99.54	53.00%	53.64	28.56%	1.57	0.84%	187.81
Total			3249.60	9.90%	7228.66	22.01%	9292.08	28.30%	8197.35	24.96%	4871.65	14.83%	32839.34

areas of 3333.73 km^2 and 1987.71 km^2, respectively, which occupy 36.61% and 21.83% of the province within the study area. Besides, the highly, moderately, and extremely vulnerable zones of Shaanxi occupy 28.06%, 11.59%, and 1.92% (174.77 km^2) of the province within the study area, respectively. Shenmu City, which is located in the northeastern part of the study area, exhibits high eco-geological vulnerability in the north, with highly vulnerable zones occupying 29.04% of the city within the study area. The highly vulnerable zones of Jingbian and Dingbian counties, which are located in the southern part of the study area, occupy 23.28% and 22.25% of the two counties within the study area, respectively. The Hengshan and Yuyang districts show significantly low vulnerability, with potentially vulnerable zones occupying 39.32% and 30.19% of the two districts within the study area, respectively (Table 9).

The Ningxia Hui Autonomous Region occupies an area of only 187.81 km^2 in the study area. It exhibits severe eco-geological vulnerability, dominated by moderately and highly vulnerable zones with areas of 99.54 km^2 and 53.64 km^2, respectively (Table 9).

5. Discussion

5.1. Eco-geological vulnerability characteristics of major land-use types

According to the statistical analysis, the grassland in the study area, covering the largest area of 16435.86 km^2, primarily shows relatively high eco-geological vulnerability and hosts the smallest area of potentially vulnerable zones among the major land-use types (Fig. 8; Table 10). The forest land, presenting a relatively extensive distribution, is dominated by moderately vulnerable zones. Unlike the grassland, the forest land has relatively high proportions of slightly and potentially vulnerable zones and the lowest proportion of extremely vulnerable zones (less than 1000 km^2). Cultivated land and other types of land exhibit similar eco-geological vulnerability trends to the forest land, with larger areas of potentially and slightly vulnerable zones compared to highly and extremely vulnerable zones. Other land in the study area is dominated by sandy land, followed by vacant land and saline-alkali land. Other land is distributed primarily in highly vulnerable zones, followed by extremely and moderately vulnerable zones, with potentially vulnerable zones covering an area less than 100 km^2. The transition from forest land to grassland and then to sandy land indicates that the composition of the ecosystem tends to be simpler, which suggests decreased ecological stability and resilience in local areas. In addition, the varying areas of cultivated land in zones with different eco-geological vulnerabilities reflect significantly different eco-geological conditions. These trends support the feasibility of the eco-geological vulnerability assessment index system proposed in this study and validate the accuracy of the assessment results.

5.2. Spatial autocorrelation analysis of eco-geological vulnerability

The results of the spatial autocorrelation analysis highlight

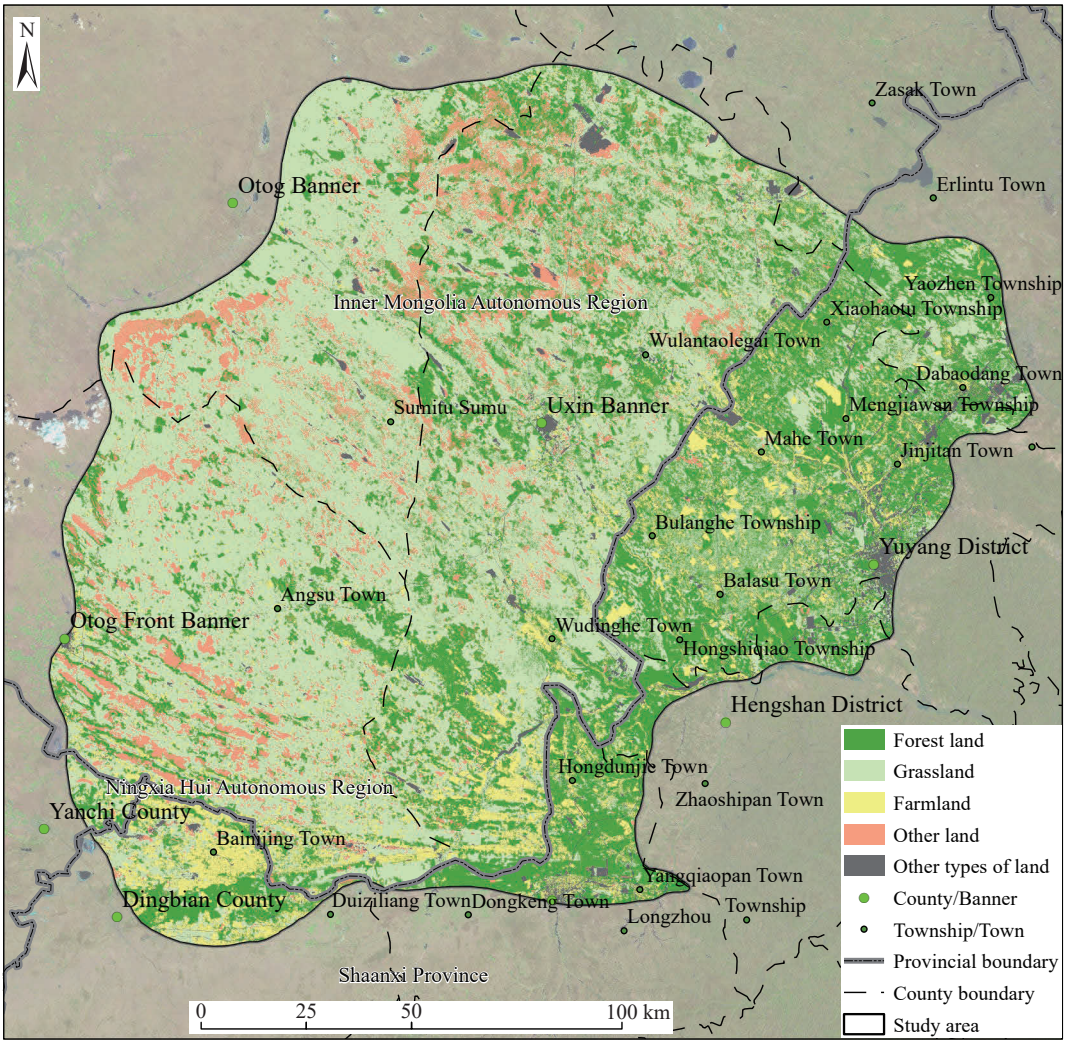

Fig. 8. Map showing the land use types of the Mu Us Sandy Land.

Table 10. Statistics of major land use types with different eco-geological vulnerabilities (km^2).

Land use type	Potentially vulnerable zones		Slightly vulnerable zones		Moderately vulnerable zones		Highly vulnerable zones		Extremely vulnerable zones		Total
Grassland	948.01	5.77%	3170.28	19.29%	4699.34	28.59%	4685.08	28.51%	2933.15	17.85%	16435.86
Forestland	1020.26	10.52%	2567.17	26.46%	3024.87	31.18%	2106.03	21.71%	984.39	10.15%	9702.71
Cultivated land	967.64	36.85%	849.72	32.36%	544.59	20.74%	218.92	8.34%	45.29	1.72%	2626.17
Other land	51.20	1.77%	286.27	9.92%	715.69	24.81%	1000.07	34.67%	831.63	28.83%	2884.87
Other types*	262.49	22.06%	355.22	29.86%	307.59	25.85%	187.24	15.74%	77.20	6.49%	1189.73
Total	3249.60	9.90%	7228.66	22.01%	9292.08	28.30%	8197.35	24.96%	4871.65	14.83%	32839.34

Note: *Other types include garden plots, commercial land, industrial and mining land, and residential land. All of them show small-scale distributions in the study area and thus are combined as one type.

that the eco-geological vulnerability is not randomly distributed, but rather exhibits significant spatial clustering. The global Moran's I index of 0.808 indicated that the eco-geological vulnerability in the Mu Us Sandy Land exhibits significantly positive spatial autocorrelations and spatial clustering (Fig. 9). Most of the data points in the study area fall in the first and third quadrants, suggesting that highly vulnerable eco-geological zones are surrounded by highly vulnerable ecological zones and that slightly vulnerable eco-geological zones are surrounded by slightly vulnerable ecological zones. These zones exhibit strongly positive correlations in eco-geological vulnerability. In addition, a small number of data points fall in the second and fourth quadrants, suggesting that slightly vulnerable eco-geological zones are surrounded by highly vulnerable eco-geological zones and that highly vulnerable eco-geological zones are surrounded by slightly vulnerable eco-geological zones. These zones exhibit negative correlations of eco-geological vulnerability.

As illustrated in the LISA clustering map depicted in Fig. 10: (1) High-high cluster zones are primarily concentrated in the northwestern part of the study area, the northern Uxin Banner -

Otog Banner - Angsu Town area, and the surrounding areas of Hondunjie Town in the southeast. These areas display a spatial distribution pattern consistent with that of the extremely vulnerable eco-geological zones. (2) Low-low

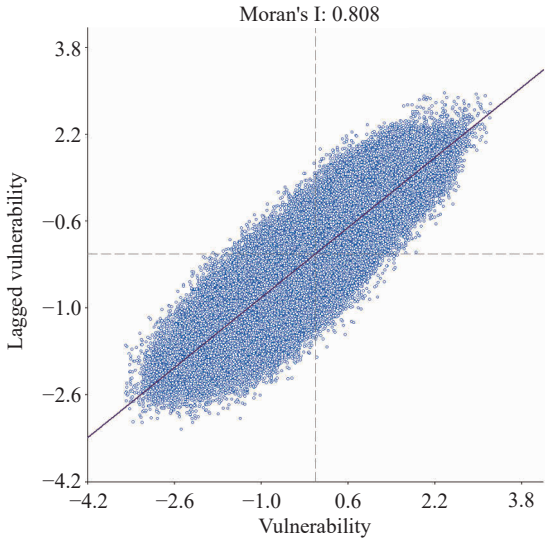

Fig. 9. Global Moran's I index of eco-geological vulnerability in the Mu Us Sandy Land.

cluster zones are primarily distributed in the Hongshiqiao Township - Xiaohaotu Township area in the eastern part of the study area, as well as in Otog Front Banner and Bainijing Town. They are spatially consistent with the distribution of slightly and potentially vulnerable zones. (3) The aforementioned zones, exhibiting positive spatial autocorrelations in eco-geological vulnerability, are significantly affected by their surrounding areas. (4) High-low and low-high outlier zones exhibit limited and scattered distributions in the study area. (5) Other zones in the study area exhibit slight clustering and significant spatial autocorrelation, with eco-geological vulnerability randomly distributed. In other words, the eco-geological vulnerability of these zones has a slight influence on the surrounding areas and also has slight effects on surrounding areas. Therefore, it is recommended that the priority of ecological conservation and restoration should be given to zones with high spatial autocorrelations, in order to increase work efficiency and rapidly improve the ecological environment.

Table 11 shows the spatial clustering characteristics of administrative areas in the study area. The specific results are as follows:

Inner Mongolia within the study area consists primarily of

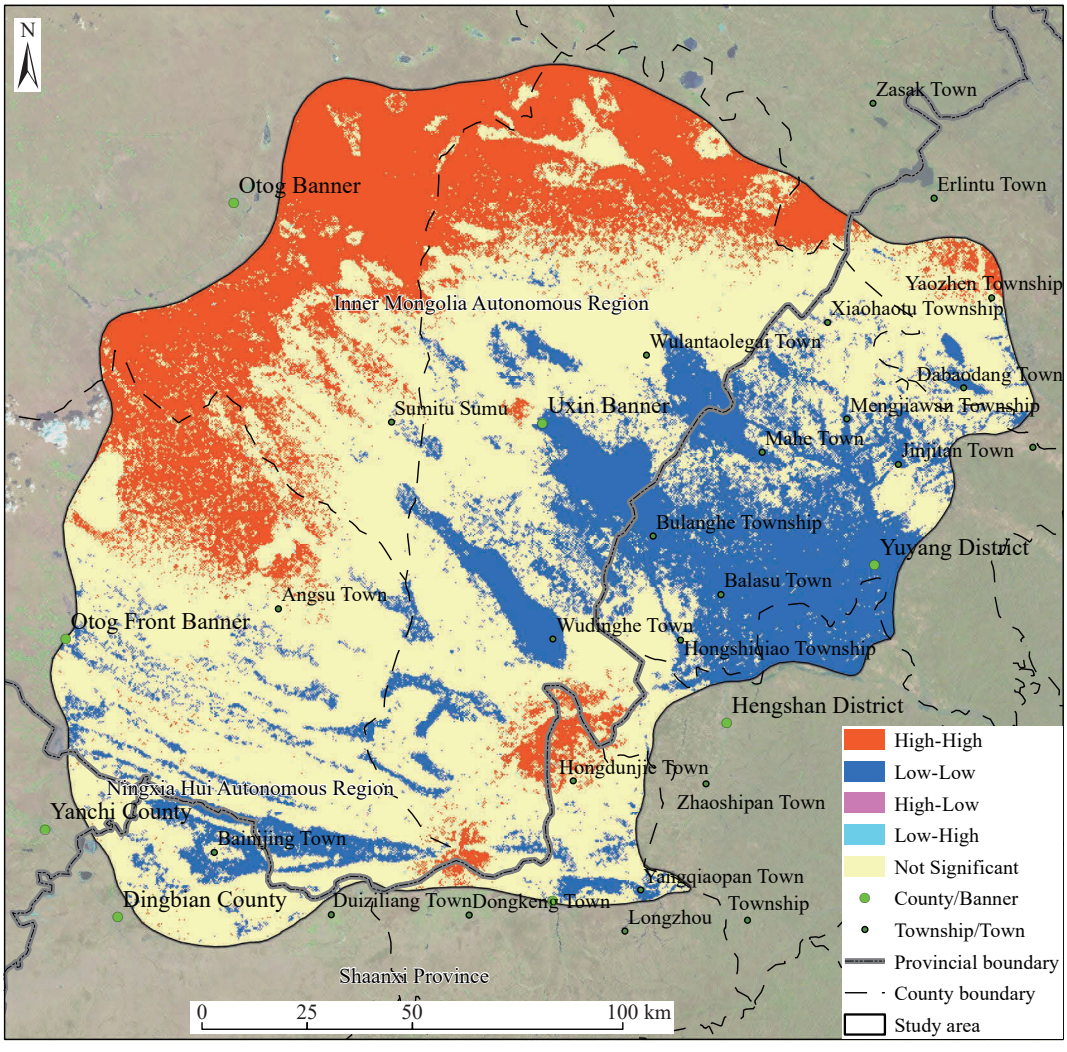

Fig. 10. LISA cluster map of eco-geological vulnerability in the Mu Us Sandy Land.

Table 11. Spatial clustering characteristics of administrative areas in the study area.

Province (autonomous region)	City	County (district or banner)	Nonsignificant		Low-low		Low-high		High-low		High-high		Total
Inner Mongolia	Ordos	Otog Banner	1830.92	36.33%	32.67	0.65%	12.59	0.25%	1.05	0.02%	3162.71	62.75%	5039.95
		Otog Front Banner	5245.87	73.78%	670.12	9.42%	13.71	0.19%	21.36	0.30%	1158.97	16.30%	7110.03
		Uxin Banner	7055.01	63.04%	1751.96	15.65%	24.70	0.22%	24.23	0.22%	2336.17	20.87%	11192.08
		Ejin Horo Banner	24.20	11.93%	0.00	0.00%	0.47	0.23%	0.00	0.00%	178.17	87.84%	202.84
Subtotal			14156.01	60.12%	2454.75	10.43%	51.48	0.22%	46.65	0.20%	6836.02	29.03%	23544.90
Shaanxi	Yulin	Dingbian County	933.99	76.48%	276.99	22.68%	0.81	0.07%	5.62	0.46%	3.78	0.31%	1221.19
		Hengshan District	223.29	32.71%	454.65	66.59%	0.09	0.01%	0.71	0.10%	3.99	0.58%	682.72
		Jingbian County	851.95	74.85%	139.32	12.24%	1.97	0.17%	4.51	0.40%	140.49	12.34%	1138.25
		Shenmu City	982.94	81.58%	100.18	8.32%	1.53	0.13%	2.89	0.24%	117.30	9.74%	1204.84
		Yuyang District	2035.76	41.89%	2801.27	57.64%	0.09	0.00%	22.50	0.46%	0.00	0.00%	4859.62
Subtotal			5027.93	55.21%	3772.41	41.42%	4.49	0.05%	36.23	0.40%	265.57	2.92%	9106.63
Ningxia	Wuzhong	Yanchi County	182.82	97.34%	3.71	1.98%	0.18	0.10%	0.47	0.25%	0.63	0.33%	187.81
Subtotal			182.82	97.34%	3.71	1.98%	0.18	0.10%	0.47	0.25%	0.63	0.33%	187.81
Total			13327.33	40.58%	9820.88	29.91%	13.5	0.04%	17.01	0.05%	9660.62	29.42%	32839.34

nonsignificant cluster zones, which cover an area of 14156.01 km^2. This region hosts extensive high-high cluster zones, with an area of 6836.02 km^2, which accounts for 29.03% of Inner Mongolia within the study area. In contrast, this region has small low-low cluster zones, with an area of 2454.75 km2, which accounts for 10.43% of Inner Mongolia within the study area. In addition, the low-high and high-low outlier zones are similar in size, accounting for 0.22% and 0.20% of Inner Mongolia within the study area, respectively. Ejin Horo Banner is dominated by high-high cluster zones, which occupy 87.84% of the banner within the study area. In Uxin Banner, high-high and low-low cluster zones account for 20.87% and 15.65% of the banner within the study area, respectively. In Otog Front Banner, nonsignificant, high-high, and low-low cluster zones occupy 73.78%, 16.30%, and 9.42% of the banner within the study area, respectively, indicating that Otog Front Banner is a transition zone for the clustering trend of eco-geological vulnerability.

Shaanxi within the study area is dominated by nonsignificant cluster zones, followed by low-low and high-high cluster zones, which occupy 55.21%, 41.42% (3772.41 km^2), and 10.66% (969.76 km^2) of the province within the study area, respectively. In addition, low-high and high-low outlier zones both account for less than 1% of the province within the study area. Among the counties or districts investigated in Shaanxi, Jingbian County hosts the largest high-high cluster zones, covering an area of 140.49 km^2, which accounts for 12.34% of the county within the study area. This county is followed by Shenmu City, whose high-high cluster zones cover an area of 117.30 km^2. Hengshan District, Yuyang District, and Dingbian County are dominated by low-low cluster zones, which account for 66.59%, 57.64%, and 22.68% of Hengshan, Yuyang, and Dingbian in the study area, respectively.

Ningxia within the study area is dominated by nonsignificant cluster zones, followed by low-low cluster zones, which occupy 97.34% and 1.98% of Shaanxi within the study area, respectively.

5.3. Suggestions for ecological conservation and restoration

The northwestern and southeastern parts of the study area are characterized by extremely vulnerable eco-geological zones and primary areas of high-high cluster zones. In the northwestern part, specifically from northern Otog Front Banner to Otog Banner, the area experiences an annual average precipitation of less than 300 mm, with an average temperature of approximately 8°C. It also has high average wind speeds exceeding 2.50 m/s and groundwater burial depths ranging from 5 m to 8 m. Additionally, this part has steep landform slopes due to the presence of large mobile dunes, which contributes to its classification as a high-high cluster zone. This part has a relatively homogeneous ecosystem dominated by grassland. With a large number of mobile dunes, this part suffers the severest sandy desertification, which is severe primarily and moderate secondarily (Liu JY et al, 2021). Therefore, the ecosystem of the northwestern part features low stability and poor self-regulation and resilience capabilities. Once the ecosystem is locally damaged, the ecological damage is prone to spread and develop into a regional problem. On the other hand, in the southeastern part of the study area, the border zone between Uxin Banner and Jingbian County the conditions are more favorable compared to the northwestern part. This border zone has higher annual precipitation, average temperature, and wind speed. However, it exhibits groundwater burial depths mostly greater than 12 m, as well as low soil fractal dimensions, and low total phosphorus and potassium contents. These factors categorize the border zone as a low-low cluster zone. Therefore, efforts to control sandy desertification in both the northwestern and southeastern parts of the study area should take into account factors such as poor meteorological conditions and deep groundwater burial depths. Moreover, it is recommended to plant drought-resistant vegetation that has reduced dependence on groundwater to mitigate the mobility of dunes and gradually restore vegetation.

The central to southwestern region within the study area is

characterized by moderately and highly vulnerable eco-geological zones, with locally slightly and potentially vulnerable eco-geological zones. This area serves as a transition zone between extremely vulnerable and slightly and potentially vulnerable zones, showing no significant spatial clustering in eco-geological vulnerability. The annual precipitation in this region is around 340 mm, with an average annual temperature of about 9°C and average wind speeds of approximately 2.30 m/s. Groundwater depths in this region are relatively shallow, with most depths being less than 3 m. Besides, the soils in this region have moderate contents of total nitrogen, total phosphorus, total potassium, and organic matter. The sandy desertification is severe in northern Uxin Banner and the border zone between Dingbian County and Otog Front Banner, resulting in numerous mobile dunes. The ecological conservation and restoration of this region should be conducted in cooperation with Otog Banner, which also suffers from severe sandy desertification, using unified methods to curb dune movement. Vegetation such as salix mongolica, which has a well-developed root system and requires certain amounts of groundwater, can be planted in this region.

The eastern part of the study area, including Yuyang District, Shenmu County, and Hengshan County, has slight eco-geological vulnerability and low-low clustering characteristics. This region experiences an annual precipitation of approximately 400 mm and has average temperatures above 9°C throughout the year. The landforms in this area are gentle with low slopes. Several rivers, such as Hailiutu, Tuwei, and Yuxi rivers, flow through the eastern part, providing abundant water resources. This part exhibits groundwater burial depths mostly less than 5 m. The field surveys show that some areas have groundwater burial depths less than 1 m, which can satisfy the water requirement of various plants, including poplar, salix matsudana, salix mongolica, sand sagebrush, and phragmites communis, thus providing sufficient water for their growth (Huang JT et al., 2008). Over the past decade, there has been a significant reduction in sandy desertification in the eastern part of the study area (Liu JY et al., 2021), indicating that the severity of desertification is relatively mild in this region. Therefore, the ecological conservation and restoration efforts in the eastern part should primarily focus on addressing severe sandy desertification in specific local areas. Meanwhile, appropriate development can be conducted concurrently, such as the development of agriculture and tourism with distinctive features of sandy land.

The specific suggestions for ecological conservation and restoration of various counties (banners or districts) in the study area are listed in Table 12.

Table 12. Suggestions for ecological conservation and restoration of various counties (banners or districts) in the study area.

County (banner or district)	Current situation of sandy desertification	Eco-geological vulnerability	Suggestions for ecological conservation and restoration
Otog Banner	Otog Banner has a sandy desertification area of 4294.18 km^2, which account for 85.20% of the banner within the study area. This banner is dominated by severe sandy desertification, which occupies 49.18% of the total desertification area.	This banner shows high eco-geological vulnerability, with the proportion of extremely vulnerable zones up to 45.65%, and feature a high-high clustering trend.	The climate in Otog Banner is arid, with limited precipitation, exacerbating the problem of sandy desertification. It is recommended that land with sandy desertification should be gradually restored from areas that can be easily restored near dune edges to more challenging areas within dunes by slowing down the dune movement using artificial sand and planting xerophytes.
Otog Front Banner	Sandy desertification are found in 92.96% of land in the Otog Front Banner in the study area, making this banner the administrative area with the highest proportion of desertification in the study area. This banner primarily shows slight sandy desertification, which accounts for 56.50 % of the total desertification area in the banner.	This banner shows relatively high eco-geological vulnerability, which is dominated by highly and moderately vulnerable zones. High-high and low-low cluster zones are situated in the northern and southern parts of the banner, respectively, showing zonal distributions.	This banner suffers relatively poor eco-geological conditions. The severe desertification is primarily concentrated in the north and south regions of the banner, aligning with the high-high cluster zones. In light of these circumstances, it would be advisable for the banner to collaborate with Otog Banner to address the severe desertification in the northern part. Utilizing techniques such as sand fencing and afforestation can help control the movement of sand dunes in the southern part of the banner. Meanwhile, it is crucial to pay attention to areas experiencing severe and moderate desertification that are scattered throughout the non-significant cluster zones. Implementing measures like grazing prohibition can help prevent the expansion of these areas.
Uxin Banner	Uxin Banner has a sandy desertification area of 10038.18 km^2, which accounts for 89.69% of the banner within the study area. This banner is dominated by moderate desertification with an area of 5026.28 km^2, which accounts for 50.07% of the sandy desertification area in this banner, followed by severe desertification.	This banner primarily shows moderate to high eco-geological vulnerability. The nonsignificant cluster zones account for 63.04% of the banner within the study area, followed by low-low and high-high cluster zones.	This banner suffers relatively poor eco-geological conditions, with the central and northern parts experiencing more severe sandy desertification compared to the southern part. Considering these circumstances, the banner should cooperate with the Otog Banner to control the sandy desertification of the high-high cluster zones in the northwestern part. The local sandy desertification in the high-high cluster zones in the southeastern part can be controlled through grazing prohibition and aerial seeding. The low-low cluster zones in the eastern part can be restored through enclosure.

Table 12. (*Continued*)

County (banner or district)	Current situation of sandy desertification	Eco-geological vulnerability	Suggestions for ecological conservation and restoration
Ejin Horo Banner	Ejin Horo Banner has a sandy desertification area of 176.87 km^2, with moderate desertification prevailing (50.07%).	This banner predominantly shows extremely severe eco-geological vulnerability, with a proportion of extremely vulnerable zones reaching 68.14%, followed by highly vulnerable zones. This banner is dominated by high-high cluster zones, which occupy 87.84% of the banner area.	This banner has a small-scale distribution within the study area. Since it has similar sandy desertification and eco-geological conditions to Uxin Banner, its ecological conservation and restoration measures can follow those to be taken in northern Uxin Banner.
Dingbian County	Dingbian County has a sandy desertification area of 553.09 km^2, which occupies 45.29% of the county within the study area. The county primarily shows slight sandy desertification.	This county is dominated by moderately vulnerable zones (38.60%), followed by slightly and highly vulnerable zones. It has widespread nonsignificant cluster zones (76.48%), followed by low-low cluster zones (22.68%).	Considering the unfavorable eco-geological conditions in this county, the ecological conservation and restoration should focus on the severe sandy desertification areas in the southern part. it is recommended for this county to collaborate with Yanchi County and Otog Front Banner to curb the sandy desertification through measures such as afforestation.
Hengshan District	Sandy desertification in the district covers an area of 475.48 km^2, dominated by slight sandy desertification (41.47%).	This district shows relatively low eco-geological vulnerability, with potentially vulnerable zones occupying 39.32% of the district area. The eco-geological vulnerability in this district exhibits low-low clustering characteristics, with low-low cluster zones occupying 66.59% of the district area.	Since this district features relatively favorable eco-geological conditions and a low sandy desertification degree, the ecological conservation and restoration should focus on the high-high cluster zones in the southern part of the district. It is necessary for this district to cooperate with Jingbian County to control sandy desertification and to protect the ecological environment of the sandy areas in the northern part of the district during development.
Jingbian County	Jingbian County has a sandy desertification area of 600.24 km^2, which accounts for 52.74% of the county within the study area. This county shows milder sandy desertification than other counties (banners or districts).	This county primarily shows moderate eco-geological vulnerability, with moderately vulnerable zones covering 36.51% of the county, followed by slightly and highly vulnerable zones. The high-high cluster zones in this county cover an area of 140.49 km^2, which accounts for 12.34% of the county.	This county has deep groundwater burial depths and low total potassium and total phosphorus contents in its soils. Given this, e ecological conservation and restoration efforts should prioritize the western and southern areas of the county. Proper utilization of water resources is crucial during the restoration process. To restore vegetation, it is recommended to plant species that are less reliant on groundwater. Aerial seeding can be used as a method for vegetation restoration.
Shenmu City	The sandy desertification in this city covers an area of 1021.06 km^2. It is dominated by moderate desertification with an area of 426.07 km^2, which accounts for 41.73% of the sandy desertification area.	This city mainly shows moderate eco-geological vulnerability. Moderately vulnerable zones account for 38.12% of the city, followed by highly and slightly vulnerable zones. Its high-high cluster zones cover an area of 117.30 km^2, which occupies 9.74% of the city.	This city has relatively normal eco-geological conditions and covers a small area. It is recommended that the high-high cluster zones in the northern region should be prioritized in collaboration with Yuyang District. In areas where there is severe sandy desertification, a combination of artificial control and natural recovery methods can be implemented as a means of restoration.
Yuyang District	The sandy desertification in this district covers an area of 3571.10 km^2. It is dominated by moderate desertification with an area of 2131.39 km^2, which accounts for 59.68% of the total sandy desertification area in this district.	This district shows low eco-geological vulnerability, which is manifested as slightly vulnerable zones (45.06%), followed by potentially vulnerable zones (30.19%). Its spatial clustering is dominated by low-low cluster zones, which account for 57.64% of the district.	The district possesses favorable eco-geological conditions; however, it is locally affected by severe sandy desertification. In light of this, ecological conservation and restoration efforts in this district should primarily emphasize natural recovery, taking full advantage of the favorable eco-geological conditions present. Additionally, the district should explore the development of agriculture and tourism industries that showcase the distinctive features of the sandy land.
Yanchi County	The sandy desertification in this country covers an area of 128.20 km^2. It is dominated by slight sandy desertification (85.24%).	The county primarily shows moderate to high eco-geological vulnerability, with nonsignificant cluster zones occupying 97.34% of the county.	The county has a small-scale distribution within the study area. Since it has similar sandy desertification and eco-geological conditions to the southern Otog Front Banner, its ecological conservation and restoration measures can follow those to be taken in the southern Otog Front Banner.

6. Conclusions

(i) Based on the results of the eco-geological survey and the ecological characteristics of the Mu Us Sandy Land, this study has developed an eco-geological vulnerability assessment index system targeting severe sandy desertification. The assessment index system involves 15 indices, including average temperature, average precipitation, average wind speed, average evapotranspiration, slope, aspect, soil parent materials, groundwater burial depth, fractal dimension, the contents of nitrogen, phosphorus, potassium, and organic matter, vegetation type, and vegetation cover. These indices are derived from five major factors, namely geology, meteorology, soil, landform, and vegetation.

(ii) This study has determined the comprehensive weights of the various indices using both the AHP and the EWM. The AHP-based weights consider expert opinions while the EWM mitigates the impact of subjective judgments by relying on data and algorithms. As a result, the assessment index system benefits from the advantages of both methods and yields more accurate and objective assessment results compared to traditional AHP-based approaches.

(iii) The Mu Us Sandy Land suffers vulnerable eco-geological conditions, with extremely and highly vulnerable zones and potentially and slightly vulnerable zones covering areas of 13069.00 km^2 (39.80% of the study area) and 10478.26 km^2 (31.91% of the study area), respectively. The extremely and highly vulnerable zones are primarily distributed in the northwestern and southeastern parts of the study area, while the potentially and slightly vulnerable zones are situated in the eastern part. Overall, the study area shows increasingly severe eco-geological vulnerability from east to west.

(iv) As revealed by the spatial autocorrelation analysis, the study area shows high spatial autocorrelations of eco-geological vulnerability. Areas with high spatial autocorrelations include the northern Uxin Banner - Otog Banner - Angsu Town area, the surrounding areas of Hongdunjie Town in the southeastern part of the study area, the Hongshiqiao Township - Xiaohaotu Township area, Otog Front Banner, and Bainijing Town. It is recommended that priority of ecological conservation and restoration efforts should be given to these zones with high spatial autocorrelations. For the northwestern part of the study area, multiple measures for ecological conservation and restoration should be taken to enhance the stability of ecosystems and mitigate the negative regional effects caused by high-high cluster zones of eco-geological vulnerability. For the eastern part of the study area, ecological conservation and restoration should focus on local areas, and appropriate development can be conducted in areas with favorable eco-geological conditions, such as the development of agriculture and tourism with distinctive features of sandy land.

This study proposes the concept of eco-geological vulnerability and establishes an assessment index system and evaluation model for the Mu Us Sandy Land, based on eco-geological surveys. However, it is important to note that some indices in the assessment index system, such as precipitation, temperature, and soil nutrients, may experience significant changes over a decade or longer. These changes could lead to variations in the assessment results of eco-geological vulnerability. Therefore, future research should focus on (1) determining a scientific time interval between assessments of eco-geological vulnerability; (2) understanding the ecological implications of changes in eco-geological vulnerability assessment results; (3) exploring the methods to conduct eco-geological vulnerability assessment under different climate zones and different ecological systems.

CRediT authorship contribution statement

Jian-yu Liu, Hong-feng Nie, Guo-li Yuan and Chun-lei Xiao conceived of the presented idea. Jian-yu Liu, Liang Xu, Wei Li, Yan-peng Huang, Xin-yang Ji and Tian-qi Li carried out the fieldwork. All authors discussed the results and contributed to the final manuscript.

Declaration of competing interest

The authors declare no conflicts of interest.

Acknowledgement

This research was jointly supported by the project of the China Geological Survey (DD20242481) and Key Laboratory of Airborne Geophysics and Remote Sensing Geology, MNR (2020YFL33).

Supplementary dataset

Supplementary data (Appendix Table 1) to this article can be found online at doi: 10.31035/cg20230027 or available on request from the authors.

References

Adger WN. 2006. Vulnerability. Global Environmental Change, 16(3), 268–281. doi: 10.1016/j.gloenvcha.2006.02.006.

Allen RG, Pereira LS, Raes D, Smith M. 1998. Crop evapotranspiration-Guidelines for computing crop water requirements-FAO Irrigation and drainage paper 56. Rome: FAO-Food and Agriculture Organization of the United Nations.

Bai GS, Li ZX, Zhang ZS. 2006. Investigation of the resources of higher plants in the Maowusu Sandy Land. Acta Agrestia Sinica, 14(2), 170–180 (in Chinese with English abstract). doi: 10.11733/j.issn.1007-0435.2006.02.016.

Buotte PC, Peterson DL, McKelvey KS. Hicke JA. 2016. Capturing subregional variability in regional-scale climate change vulnerability assessments of natural resources. Journal of Environmental Management, 169(15), 313–318. doi: 10.1016/j.jenvman.2015.12.017.

Cheng DH, Wang WK, Hou GC, Yang HB, Li Y, Zhang E. 2012. Relationship between vegetation and groundwater in Mu Us Desert. Journal of Jilin University (Earth Science Edition), 42(1), 184–189 (in Chinese with English abstract). doi: 10.13278/j.cnki.jjuese.2012.01.026.

Dückers M, Frerks G, Birkmann J. 2015. Exploring the plexus of context and consequences: An empirical test of a theory of disaster vulnerability. International Journal of Disaster Risk Reduction, 13, 85–95. doi: 10.1016/j.ijdrr.2015.04.002.

Eimil-Fraga C, Rodríguez-Soalleiro R, Sánchez-Rodríguez F, Pérez-Cruzado C, Álvarez-Rodríguez E. 2014. Significance of bedrock as a site factor determining nutritional status and growth of maritime pine. Forest Ecology and management, 331, 19–24. doi: 10.1016/j.foreco.2014.07.024.

Frigerio I, Ventura S, Strigaro D, Mattavelli M, De Amicis M, Mugnano S, Boffi M. 2016. A GIS-based approach to identify the spatial variability of social vulnerability to seismic hazard in Italy. Applied Geography, 74, 12–22. doi: 10.1016/j.apgeog.2016.06.014.

Hahm WJ, Riebe CS, Lukens CE, Araki S. 2014. Bedrock composition regulates mountain ecosystems and landscape evolution. Proceedings of the National Academy of Sciences, 111(9), 3338–3343. doi: 10.1073/pnas.1315667111.

He L, Shen J, Zhang Y. 2018. Ecological vulnerability assessment for

ecological conservation and environmental management. Journal of Environmental Management, 206, 1115–1125. doi: 10.1016/j.jenvman.2017.11.059.

He TH. 2009. The Environment Change Of Mu Us Desert In Historical Period. Lanzhou University. Ph. D thesis, 12–13 (in Chinese with English abstract).

He ZW, Huang RQ, Sun CM, Wu BQ, Han LL, He FQ, Sun YJ, Yin JZ, Liu SJ, Zhao YB. 2003. A brief discussion on "Eco-Geology". Scientific and Technological Management of Land and Resources, 3, 69–72 (in Chinese with English abstract).

Hong WY, Jiang RR, Yang CY, Zhang FF, Su M, Liao Q. 2016. Establishing an ecological vulnerability assessment indicator system for spatial recognition and management of ecologically vulnerable areas in highly urbanized regions: A case study of Shenzhen, China. Ecological Indicators, 69, 540–547. doi: 10.1016/j.ecolind.2016.05.028.

Hu XJ, Ma C, Huang P, Guo X. 2021. Ecological vulnerability assessment based on AHP-PSR method and analysis of its single parameter sensitivity and spatial autocorrelation for ecological protection-A case of Weifang City, China. Ecological Indicators, 125, 107464. doi: 10.1016/j.ecolind.2021.107464.

Huang JT, Hou GC, Tao ZP, Zhao ZH, Wang XY, Cui XD. 2008. Vegetation ecological areas of the Ordos Plateau, China and their hydrogeological significance. Geological Bulletin of China, 27(8), 1330–1334 (in Chinese with English abstract).

Huang YF, Li FL, Bai XM, Cui SH. 2012. Comparing vulnerability of coastal communities to land use change: Analytical framework and a case study in China. Environmental Science & Policy, 23, 133–143. doi: 10.1016/j.envsci.2012.06.017.

Jewitt D, Erasmus B, Goodman PS, O'Connor TG, Hargrove WW, Maddalena DM, Witkowski ETF. 2015. Climate-induced change of environmentally defined floristic domains: A conservation based vulnerability framework. Applied Geography, 63, 33–42. doi: 10.1016/j.apgeog.2015.06.004.

Jiang ZH, Liu HY, Wang HY, Peng J, Meersmans J, Green SM, Quine TA, Wu XC, Song ZL. 2020. Bedrock geochemistry influences vegetation growth by regulating the regolith water holding capacity. Nature Communications, 11(1), 2392. doi: 10.1038/s41467-020-16156-1.

Lee YJ. 2014. Social vulnerability indicators as a sustainable planning tool. Environmental Impact Assessment Review, 44, 31–42. doi: 10.1016/j.eiar.2013.08.002.

Li C. 2019. Monitoring and analysising of desertification in Mu Us Sandy land based on differential index. East China Institute of Technology. Master thesis, 9–10 (in Chinese with English abstract).

Li PX, Fan J. 2014. Regional ecological vulnerability assessment of the Guangxi Xijiang River Economic Belt in Southwest China with VSD Model. Journal of Resources & Ecology, 5(2), 163–170. doi: 10.5814/j.issn.1674-764X.2014.02.009.

Li ZX, Liao YC, Bai GS. 2005. Characteristic and construction of vegetation in Maowusu Sandy Land. Bulletin of Soil and Water Conservation, 25(5), 70–74,78 (in Chinese with English abstract). doi: 10.13961/j.Cnki.Stbctb.2005.05.016.

Liu JY, Nie HF, Song BF, Xiao CL, Yuan GL, Shang BX, Pan Z. 2024. The wind erosion, land desertification and ecogeological effects in the northern piedmont of Yinshan Mountain in Inner Mongolia. Geology in China, 51(3), 1020–1033. DOI: 10.12029/gc20210607002. (in Chinese with English abstract).

Liu JY, Nie HF, Xiao CL, Shang BX, Li W, Ji XY. 2021. Evolution of sandy desertification in North China from 2010 to 2018. Geology Survey in China, 8(6), 25–34 (in Chinese with English abstract). doi: 10.19388/j.zgdzdc.2021.06.03.

Liu QQ, Yang XQ. 2018. Geochemical composition and provenance of aeolian sands in the Ordos Deserts, northern China. Geomorphology, 318, 354–374. doi: 10.1016/j.geomorph.2018.06.017.

Liu Z, Huang XK, Xu HL, Zhang B, Peng QS, Wang CS, Wang H, Jiang H. 2020. Migration characteristics of elements in the rock-soil system and suitability evaluation of orange planting in Yaqueling area, Yichang, Hubei Province. Geology in China, 47(6), 1853–1868 (in Chinese with English abstract). doi: 10.12029/gc20200620.

Lu HY, Miao XD, Zhou Y, Mason J, Swinehart J, Zhang J, Zhou L, Yi S. 2005. Late Quaternary aeolian activity in the Mu Us and Otindag dune fields (north China) and lagged response to insolation forcing. Geophysical Research Letters, 32(21), 716. doi: 10.1029/2005GL024560.

Luo RY, Zhang SR, Xu XX, Li T. 2015. Profile distribution characteristics of soil organic nitrogen fractions in the lower reaches of the Heihe River wetland. Acta Ecologica Sinica, 35(4), 956–964 (in Chinese with English abstract). doi: 10.5846/stxb201305191113.

Ma Z, Xia YB, Li HT, Han B, Yu XZ, Zhou YL, Wang YS, Guo X, Li HQ, Pei YD. 2021. Analysis of natural resources and environment eco-gmeological conditions in the Xiong'an New Area. Geology in China, 48(3), 677–696 (in Chinese with English abstract). doi: 10.12029/gc20210301.

Mao L. 2019. Correlation of Soil Grain Size and Organic Matter in Different Land Types in Mu Us Sandland. Shanxi University. Master thesis, 11–12 (in Chinese with English abstract).

Martin V. 2008. The vulnerable can't speak. An integrative vulnerability approach to disaster and climate change research. Behemoth: A Journal on Civilisation, 1(3), 39–56. doi: 10.1524/behe.2008.0022.

Nie HF, Xiao CL, Dai M, Liu JY, Shang BX, Guo ZC, He P, OY Y, Lei TC, Li WM, Zhou CF, Jiang QG. 2021a. Progresses and main achievements of ecogeological survey project. Geology Survey in China, 8(1), 1–12. doi: 10.19388/j.zgdzdc.2021.01.01.

Nie HF, Xiao CL, Ren WX, Liu JY, Dai M. 2021b. Progress and prospect of ecogeological research. Geology Survey in China, 8(6), 1–8 (in Chinese with English Abstract). doi: 10.19388/j.zgdzdc.2021.06.01.

Santos RG, Sturaro JR, Marques ML, Faria TT. 2015. GIS applied to the mapping of land use, land cover and vulnerability in the outcrop zone of the Guarani Aquifer System. Procedia Earth and Planetary Science, 15, 553–559. doi: 10.1016/j.proeps.2015.08.099.

Shahbazi F, Jafarzadeh AA, Shahbazi MR. 2009. Agro-ecological field vulnerability evaluation and climate change impacts in Souma area (Iran), using MicroLEIS DSS. Biologia, 64, 555–559. doi: 10.2478/s11756-009-0104-9.

Shao HY, Sun XF, Wang HX, Zhang XX, Xiang ZY, Tan R, Chen XY, Xian W, Qi JG. 2016. A method to the impact assessment of the returning grazing land to grassland project on regional eco-environmental vulnerability. Environmental Impact Assessment Review, 56, 155–67. doi: 10.1016/j.eiar.2015.10.006.

Tan SJ. 2018. The study of ecological suitability evaluation and layout of land consolidation projects: A case of Dianjiang County in Chongqing City. Chongqing, Chongqing Normal University, Master thesis, 37–38 (in Chinese with English Abstract).

Tánago IG, Urqiujo J, Blauhut V, Villarroya F, Villarroya LD. 2016. Learning from experience: A systematic review of assessments of vulnerability to drought. Natural Hazards, 80, 951–973. doi: 10.1007/s11069-015-2006-1.

Timmerman, P. 1981. Vulnerability, Resilience and the Collapse of Society: A Review of Models and Possible Climatic Applications. Toronto, Canada: Institute for Environmental Studies, University of Toronto.

Trofimov VT. 2001. Ecological geology a novel branch of geological science. Earth Science Frontiers, 8(1), 27–35.

Trofimov VT. 2004. Approaches, principles and criteria of evaluation of ecological geology conditions. Earth Science Frontiers, 11(2), 533–542.

Trofimov VT. 2008. Ecological geology, environmental geology, geoecology: Contents and relations. Moscow University Geology Bulletin, 63, 59–69. doi: 10.3103/S0145875208020014.

Turner BL, Kasperson RE, Matson PA, McCarthy JJ, Corell RW, Christensen L, Eckley N, Kasperson JX, Luers A, Martello ML, Polsky C, Pulsipher A, Schiller A. 2003. A framework for vulnerability analysis in sustainability science. Proceedings of the National Academy of Sciences. 100(14), 8074–8079. doi: 10.1073/pnas.1231335100.

Tyler SW, Wheatcraft SW. 1992. Fractal scaling of soil particle-size distributions: Analysis and limitations. Soil Science Society of America Journal, 56(2), 362–369. doi: 10.2136/sssaj1992.03615995005600020005x.

Vaidya OS, Kumar S. 2006. Analytic hierarchy process: An overview of applications. European Journal of Operational Research, 169(1), 1–29. doi: 10.1016/j.ejor.2004.04.028.

Wang CS, Wang DK. 1997. On 1: 50, 000 Ecological Geological invesitgation. Regional Geology of China, 16(1), 57–60 (in Chinese with English Abstract).

Wang JB, Wei XF, Zhang HQ, Gan FW. 2020. The eco-geological survey based on geological formation, exemplified by integrated geological survey of National Ecological Civilization Demonstration Area in Chengde City, Hebei Province. Geology in China, 47(6), 1611–1624 (in Chinese with English abstract). doi: 10.12029/gc20200601.

Wang KF, LI Na, Yu XF, Wang YL, Liu Yang. 2014. The construction and application of the index system of eco-environmental carrying capacity in Shandong peninsula. Geology in China, 41(3), 1018–1027. (in Chinese with English abstract).

Wang Q, Lu C, Fan ZP. 2017. River habitat quality assessment based on principal component analysis and entropy weight in Qinghe River as a case. Ecological Science, 36(4), 185–193 (in Chinese with English abstract).

Williams LR, Kapustka LA. 2000. Ecosystem vulnerability: A complex interface with technical components. Wiley Online Library, 19(4), 1055–1058. doi: 10.1002/etc.5620190435.

Xue LQ, Wang J, Zhang LC, Wei GH, Zhu BL. 2019. Spatiotemporal analysis of ecological vulnerability and management in the Tarim River Basin, China. The Science of the Total Environment, 649, 876–888. doi: 10.1016/j.scitotenv.2018.08.321.

Yan X, An H. 2017. Fractal features of soil particle size in the process of desertification in desert grassland of Ningxia, China. Chinese Journal of Applied Ecology, 28(10), 3243–3250 (in Chinese with English abstract). doi: 10.13287/j.1001-9332.201710.024.

Yang SW, Dong B, Liu LP, Sun L, Sheng SW, Wang Q, Peng WJ, Wang X, Zhang ZF, Zhao J. 2015. Research on vegetation coverage change in Sheng Jin Lake Wetland of Anhui Province. Wetlands 35, 677–682. doi: 10.1007/s13157-015-0657-z.

Yu N. 2018. Spatiotemporal Patterns of Ecosystem Services and Influencing Factors in the Mu Us Sandy Land. Beijing, Beijing Forestry University, Master thesis, 10–11 (in Chinese with English Abstract).

Zang Z, Zou XQ, Zuo P, Song QC, Wang CL, Wang JJ. 2017. Impact of landscape patterns on ecological vulnerability and ecosystem service values: An empirical analysis of Yancheng Nature Reserve in China. Ecological Indicators, 72, 142–152. doi: 10.1016/j.ecolind.2016.08.019.

Zhang F, Liu XP, Zhang JQ, Wu R, Ma QY, Chen YN. 2017. Ecological vulnerability assessment based on multi-sources data and SD model in Yinma River Basin, China. Ecological Modelling, 349, 41–50. doi: 10.1016/j.ecolmodel.2017.01.016.

Zhang JH, Ouyang Y, Liu Hong, Huang HX, Zhang TJ, Li F, Li T. 2021a. Eco-geological vulnerability assessment based on major controlling factors: A case study of Xichang City, Sichuan Province. Remote Sensing for Natural Resources, 33(4), 181–191 (in Chinese with English abstract). doi: 10.6046/zrzyyg.2021012.

Zhang JH, Ouyang Y, Chen YZ, Li F, Liu XX, Liu H, Zhao YB. 2021b. Land suitability evaluation of agricultural industrial park based on UAV remote sensing in Zhaojue County of Sichuan Province. Geology in China, 48(6), 1710–1719 (in Chinese with English abstract). doi: 10.12029/gc20210604.

Zhang JR, Zhu RG, Zhu WH. 2004. Fractal features of soils characterized by grain size distribution. Journal of Hydraulic Engineering, 6, 69–73,81 (in Chinese with English Abstract). doi: 10.13243/j.cnki.sl xb.2004.04.012.

Zhang L. 2021. Studies on community characteristics and ecosystem services of shrub plantation in Mu Us Sandy Land. Hohhot, Inner Mongolia University, Ph. D thesis, 16–18 (in Chinese with English abstract).

Zhang XQ, Wang LK, Fu XH, Li H, Xu CD. 2017. Ecological vulnerability assessment based on PSSR in Yellow River Delta. Journal of Cleaner Production, 167, 1106–1111. doi: 10.1016/j.jclepro.2017.04.106.

Zhang XS. 2007. Vegetation Map of the People's Republic of China (1∶1000000). Beijing, Geology Press.

Zhao JC, Ji GX, Tian Y, Chen YL, Wang Z. 2018. Environmental vulnerability assessment for mainland China based on entropy method. Ecological Indicators, 91, 410–422. doi: 10.1016/j.ecolind.2018.04.016.

Zhao L, Zhang DR, Huang JT, Jin XM, Du XX, Tian XZ. 2012. Research on soil water distribution around Salix psammophila in the semi-arid and semi-desert area. Journal of Water Resources & Water Engineering, 23(5), 63–66 (in Chinese with English abstract).

Zhao M, Wang WK, Wang ZF, Chen L, Ma YT, Song H. 2018. Biomass of Artemisia ordosica in sand land and its root system distribution characteristics in the semiarid regions. Acid Land Geography, 41(4), 786–792 (in Chinese with English abstract). doi: 10.12118/j.issn.1000-6060.2018.04.14.